REACTIVITY AND CONTINUED ACTIVITY OF IMMOBILIZED ZINC OXIDE NANOPARTICLES ON METHYL PARATHION DECONTAMINATION

A Thesis

Presented to the Faculty of the Graduate School

of Cornell University

In Partial Fulfillment of the Requirements for the Degree of

Master of Science

By Yunfei Han

May 2014

ABSTRACT

Photocatalytic degradation activity and reusability of ZnO nanoparticles and immobilized ZnO in polyacrylonitrile (PAN) nanofibers were investigated. It was found that photocatalytic degradation using ZnO is a rapid and effective way to degrade methyl parathion. The photocatalytic degradation reactivity of ZnO nanoparticles remained in four cycles with some loss of activity, while the photocatalytic degradation reactivity of ZnO/PAN nanofibers remained in five cycles with no loss of activity detected. By analyzing samples using HPLC chromatograms, mass spectra, UV-vis spectra, calculated octanol-water partition coefficients, and ^{31}P NMR spectrum, it was shown that the possible mechanism of the photocatalytic degradation in water/ethanol is predominated by hydrolysis.

BIOGRAPHICAL SKETCH

Yunfei Han was born and raised in Shanghai, P.R. China. Before beginning her M.S. study in Fiber Science program at Cornell University, she earned a B.E. degree in the field of Textile Science and Engineering from Donghua University, Shanghai, P. R. China. During her undergraduate study, she spent her senior year in UC Davis as an exchange student studying courses in Textile Chemistry and doing research in the field of surface modification on fibrous membranes. Her specific research activities at Cornell involves development of high performance polymer nanofibers that is able to decontaminate chemical and biological warfare, electrospinning, and interpretation of data using statistical methods. She completed her M.S. in Fiber Science in 2014.

To my parents

ACKNOWLEDGMENTS

I first and foremost I would like to express my sincere thanks to Professor S. Kay Obendorf, my research advisor, for her constant guidance, encouragement, and understanding that made this work possible.

Professor Anil Netravali, for serving on my special committee and for his kind suggestions.

Dr. Xia Zeng, Lab Manager in Fiber Science Department of Cornell, for his technical supports and equipment training. Dr. John Hunt and Dr. Don Werder of Cornell Center for Materials Research (CCMR) for their technical supports on SEM equipment.

The research group members, Laura Lange and Nancy Elizabeth Allen, for their generous help and warm friendship.

My very special thanks go to my parents, who are always there for me. Their endless love and never failing support encourage and motivate me, which led me through to the end of this journey.

This research was funded by America Association of Textile Chemists and Colorists (AATCC) and the College of Human Ecology, Cornell University.

TABLE OF CONTENTS

LIST OF FIGURES

LIST OF TABLES

LIST OF SCHEMES

1. Abstract

Photocatalytic degradation activity and reusability of ZnO nanoparticles and immobilized ZnO in polyacrylonitrile (PAN) nanofibers were investigated. It was found that photocatalytic degradation using ZnO is a rapid and effective way to degrade methyl parathion. The photocatalytic degradation reactivity of ZnO nanoparticles remained in four cycles with some loss of activity, while the photocatalytic degradation reactivity of ZnO/PAN nanofibers remained in five cycles with no loss of activity detected. By analyzing samples using HPLC chromatograms, mass spectra, UV-vis spectra, calculated octanol-water partition coefficients, and ^{31}P NMR spectrum, it was shown that the possible mechanism of the photocatalytic degradation in water/ethanol is predominated by hydrolysis.

2. Introduction

Chemical or biological warfare (CBW) agents have increasingly threatened military, professional workers, farmers and normal people's lives since World War I [1]. Protection gear and apparel are urgently needed for both the military and professional workers. In recent years, U.S. Government has expended intensive efforts to protect military and residents from CBW agents. Military protective garments that provide the most protection against CBW agents are made of unbreathable polymer films that act as physical barriers [2]. These garments can block toxic chemicals and bacteria as well as moisture and airflow, which makes them very uncomfortable to wear. To overcome these disadvantages, permeable suits was invented with porous materials which was able to absorb the CW agents while allow air to flow through the porous structure [3]. However, toxic residual on both unbreathable and permeable garment might cause severe risk and environment pollution.

Other than physical barriers, chemical decontamination is a way to directly decompose CBW agents into non-toxic compounds. Researchers have proven that some powerful chemical can decontaminate CBW agents [4], but most of these chemical agents are extremely strong oxidants that can be hazardous. In some situations, special equipment such as heater and plasma decontamination chambers [5, 6] is required to decontaminate CBW agents. Since military apparel requires

properties of breathability, durability, washability as well as self-detoxification ability, most of these methods are not suitable.

Photocatalysis has attracted attention as a low cost, harmless, effective oxidation process for pollutants. Almost all types of organic substances can be degraded by photocatalysis [7, 8]. Photocatalyst, especially TiO_2 has been broadly studied for almost four decades [9]. Semiconductors such as Si, TiO_2, ZnO, WO_3, CdS, ZnS, $SrTiO_3$, SnO_2, WSe_2, Fe_2O_3 act as photocatalysts [7]. In this study, ZnO was chosen as the photocatalyst for the following reasons : (1) ZnO is a good antibacterial material [10, 11]; (2) No significant effort has been made in evaluating the photocatalytic efficiency ZnO for self-decontamination of protective clothing.

Methyl parathion, a toxic organophosphate widely used as a CBW agent and pesticide, was the model toxic chemical in this research. It is classified by World Health Organization (WHO) as extremely hazardous (Class IA) [14]. Fig. 2.1 shows the structure of methyl parathion.

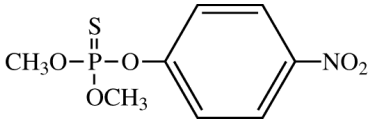

Figure 2.1 Chemical structure of methyl parathion

The purpose of this work is to create a washable and reusable nano-scale fiber that is capable of decontaminating CBW agent, to understand the photocatalytic decontamination pathway of methyl parathion, to investigate the reactivity of

photocatalytic decontamination of methyl parathion by ZnO nanoparticles and ZnO/PAN nanofibers, and to evaluate the reusability of ZnO nanoparticles and ZnO/PAN nanofibers for methyl parathion decontamination. ZnO nanoparticles were immobilized in polyacrylonitrile (PAN) nanofibers by electrospinning to evaluate self-decontamination and reuse activity.

In this thesis (Scheme 2.1), reactivity of ZnO nanoparticles on methyl parathion with and without UV was tested by LC-MS/DAD. Based on the data from LC-MS/DAD and NMR and calculated solubility and octanol-water partition coefficient data of possible degradation products, a tentative degradation pathway under hydrolytic conditions was developed. Then, continued activity of ZnO nanoparticles on methyl parathion was investigated. In the later part of the thesis, electrospun ZnO/PAN fibers were created and decontamination reactivity and decontamination reusability of the nanofibers with multiple cycles were investigated.

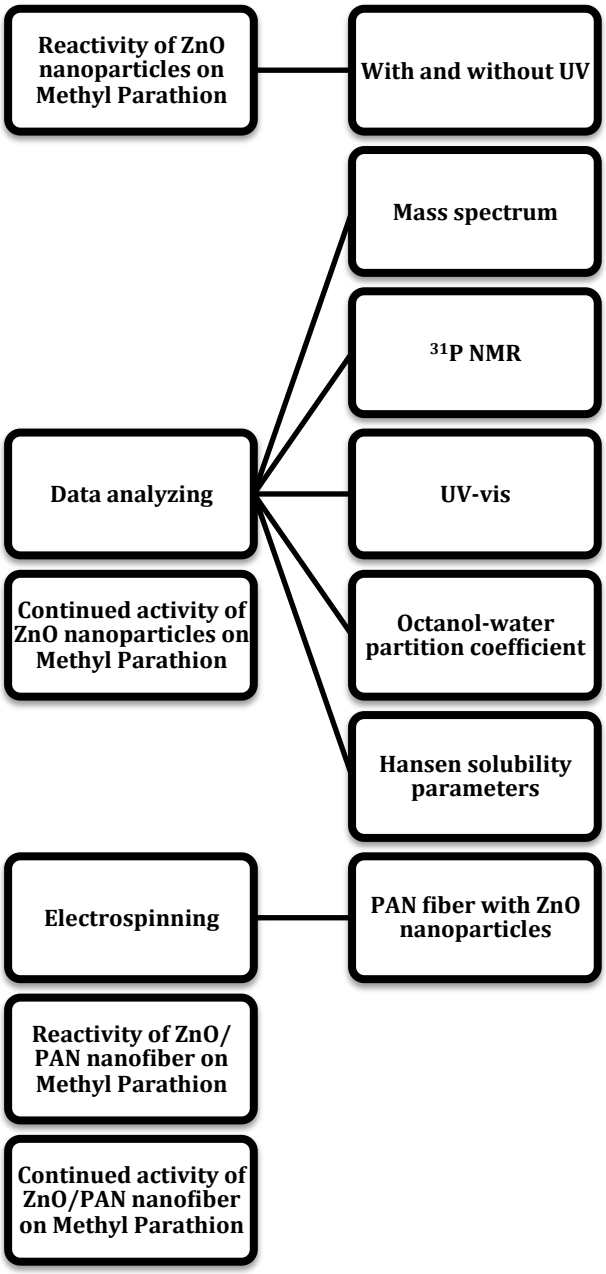

Scheme 2.1 Flowchart of the thesis process

3. Review of Literature

3.1 Zinc Oxide

Among the 3d transition metal oxide semi-conductor series, ZnO and TiO_2 are two metal oxides that have stability in photo-excitation state. The photocatalytic property of TiO_2 has been investigated in toxic chemical degradation. However, little significant effort has been made in evaluating the photocatalytic efficiency of ZnO for use in protective clothing materials, which is the major reason that ZnO was chosen as the photocatalyst in this study. The band gap energy of ZnO is 3.37 eV, which provides it remarkable application potential in areas such as solar cells, sensors, displays, gas sensors, varistors, photo-diodes and UV light emitting devices, sun-screens, gas sensors, UV absorbers, anti-reflection coatings, and photo-catalysis [15].

ZnO is also effective as an antibacterial agent. Liu et al. [16] found ZnO to have antibacterial activity against *Escherichia coli*. Their results indicate that ZnO nanoparticles may distort and damage bacterial cell membrane, consequently resulting in leakage of intracellular contents and eventually the death of bacterial cell. Yamamoto [17] investigated the antibacterial activity on *Staphylococcus aureus* and *Escherichia coli*. He discovered that the influence of ZnO on *Staphylococcus aureus* was less than that for *Escherichia coli*. In continued investigation of the effect of ZnO lattice constant on antibacterial characteristics, he found that the

antibacterial activity of ZnO increased with the increase of lattice constant value [18]. ZnO nanoparticles also have been shown to have antibacterial activity against *Campylobacter jejuni* [19]. Recently, ZnO-modified hybrid polymers were used as an antibacterial finish for textile [11].

ZnO powder has been used as sunblock for over a century. Sunscreens containing physical blockers (ZnO, TiO_2) of UV have been shown to be highly effective in protecting cells against UV-induced DNA damage [21]. Research publications by Mitchnick et al. [22] and Pinnell et al. [23] show that ZnO absorbs UV more effectively than TiO_2. Thus, by putting ZnO into protective clothing materials, anti-bacterial, sun-blocking properties as well as the self-decontamination property investigated in the current study may all be achieved. Lee [24] developed a layered fabric system with electrospun polyurethane/ZnO nanocomposite fibers and demonstrated the feasibility of antimicrobial and UV-protection multi-functionality.

3.2 Photocatalysis

The current study was based on the mechanism of photocatalysis reaction, by which toxics pollutants as well as chemical warfare agents are degraded into non-toxic compounds such as water and CO_2 [25]. ZnO was chosen as the photocatalyst in the study based on its properties discussed in section 3.1.

3.2.1 Mechanism

Photocatalytic reaction is initiated when ultraviolet (UV) or near-ultraviolet photons are released on a semiconductor catalyst. Electrons (e^-) are excited by the energy from the valence band to the conduction band, thus positive holes (h^+) are generated in the valence band. Those electrons and holes migrate to the surface of photcatalyst. Most of the electron-hole pairs (e^--h^+ pair) combine in a few nanoseconds after their migration to the surface of photocatalyst, and thermal energy is generated. Oxidation and reduction reactions are initiated by the rest of the e^- and h^+ [26-28]. The free e^- combine with O_2 and become super oxide anions ($O_2^{\bullet -}$). Through the formation of $HO_2\bullet$ radicals and H_2O_2, $O_2^{\bullet -}$ are further converted to strong oxidizing hydroxyl radicals ($HO\bullet$). Similarly, the positive holes (h^+) on the surface of the photocatalyst take electrons from H_2O and becomes $HO\bullet$ [26-28]. It is generally considered that $HO\bullet$ is the major radical species that contribute in photocatalysis [28]. Thus, by oxidation and/or hydrolysis, hazardous CBW agents can be degraded into water, CO_2 or other less harmful compounds. The above photocatalystic process can be described via the following reaction equations:

$$ZnO \xrightarrow{hv} (e^-) + (h^+) \quad (1)$$

$$(e^-) + (h^+) \rightarrow heat \quad (2)$$

$$(h^+) + H_2O_{ads} \rightarrow HO^\bullet + H^+ \quad (3)$$

$$(h^+) + 2HO^-_{ads} \rightarrow HO^\bullet + HO^- \quad (4)$$

$$(e^-) + O_{2ads} \rightarrow O_2^{\bullet} \quad (5)$$

$$O_2^{\bullet -} + H^+ \rightarrow HO_2^{\bullet} \quad (6)$$

$$O_2^{\bullet -} + HO_2^{\bullet} + H^+ \rightarrow O_2 + H_2O_2 \quad (7)$$

$$H_2O_2 + H^+ + (e^-) \rightarrow HO^{\bullet} + H_2O \quad (8)$$

$$\text{Organic compound} + HO^{\bullet} \rightarrow \text{Intermediate organic products} \quad (9)$$

$$\text{Intermediate organic products} + HO^{\bullet} \rightarrow CO_2 + H_2O \quad (10)$$

where *ads* represents an adsorbed organic molecule [26-28].

3.2.2 Challenges in Photocatalytic Decontamination

3.2.2.1 Loss of catalyst particles and introduction of the new pollutant

The most widely applied photocatalysts for decontamination in liquid system are TiO_2 and ZnO. These fine particles have mostly been applied in a suspending status for water purification. With the slurry TiO_2 or ZnO system, loss of catalyst particles and introduction of the new pollutant in the treated solution may happen during the separation process. A post-separation step would need to be conducted to recycle the photocatalytic particles. Processing hybridization with conventional sedimentation [29], cross-flow filtration [30], and various membrane filtrations [31,32] were previously studied as separation methods. However, all of the above separation method require precision operation during the process or some particles may remain in the solution. Woo et al. [33] immobilized TiO_2 nanoparticles for fixation in fibers by electrospinning; Lee [24] developed a layered fabric systems

based on electrospun polyurethane/ZnO nanocomposite fibers, which immobilized the particles and limited their release as a new pollutant.

3.2.2.2 Fouling

Fouling is the accumulation of unwanted material on solid surfaces to the detriment of function. Fouling phenomena are common and diverse. In photocatalytic reactions, fouling may occur on the surface of photocatalyst during the degradation process by adsorbing pollutes or degradation products [35]. Most photocatalysts can be reused and their decontamination activity recovered, but fouling may reduce the surface area that can be activated by UV, thus decrease decontamination efficiency. Several methods have been developed to prevent the fouling or pore blocking such as washing [36], direct contact membrane distillation [37], cooperating inorganic ions [38], or immobilizing catalysts onto active carbon [39], mesoporous clays [40] or fibers [41].

Only a few reports regarding fouling and its removal on ZnO surface have been previously published. Fiermans et al. [42] developed a method of chemical etching and annealing under ambient conditions as a cleaning method of ZnO single crystals. However, Coppa et al. [43] found that annealing ZnO in pure oxygen reduced but did not eliminate all detectable hydrocarbon contaminates. Meng et al. [44] detected carbon contamination on ZnO surface by XPS, and the removal of the contamination was achieved by 5-minutes Ar-ion bombardment. In a study by Leschkies et al. [45], ZnO nanowires were exposed to oxygen plasma to remove surface-bound

contaminants such as hydroxyl and hydrocarbon groups. It is also worth mentioning that ZnO itself has been largely used as an antifouling-coating composition for use on the surface of materials such as fishnets, water conduits and boat hulls, shower curtains, hospital walls, and roofs [46].

3.3 Chemical and Biological Warfare

In addition to nuclear, chemical and biological warfare (CBW) agents are weapons of mass destruction. The first use of toxic gas on the war front was on 22 April 1915, by the Germans, against Canadian and French colonial troops. In World War I, at least 1.3 million people, including Adolf Hitler, were killed or wounded by gas, and almost 100 thousand of them died [47]. In the 1930s, Japan launched more than 800 CBW agents in its conquest of Manchuria, China. The Japanese also are believed to have conducted experiments with those agents on thousands of Chinese prisoners of war [47]. In World War II, the Germans developed tabun and sarin, and their factories were capable of producing 11000 tons of hazardous gas per month. The British and United States also actively developed CBW at that time. Britain had actually produced 5 million cattle cakes filled with anthrax, and the United Sates had a possible plan to use the anthrax bomb against Germany [47].

3.3.1 Biological Warfare

Biological warfare (BW) agents include bacterial agents, viral agents and biological toxins [48]. Bacteria are small, single-celled organisms, many of which

grow on solid or liquid media. Viruses are a simple type of microorganism that consist of a capsid containing a protein coat containing genetic material of nucleic acid, either RNA (ribonucleic acid) or DNA (deoxyribonucleic acid). Biological toxins can cause significant illness at very low concentrations. As a result, they are mostly appealing as bioterrorism rather than for their lethality. [48]

3.3.2 Chemical Warfare

Unlike BW agents, chemical warfare (CW) agents are usually more toxic. They are defined as chemical substances that are intended for use in warfare or terrorist activities to kill, seriously injure, or seriously incapacitate people through their physiological effects [49]. Blister agents, nerve gases, choking agent, asphyxiants, and behavioral altering agents are five classifications of CW agents [49]. Blister agents are chemicals that cause severe blistering when in contact with skin. Sulfur mustard, nitrogen mustard, and lewisite are classified as blister agents. Nerve agents are organophosphorus compounds that are capable of inhibiting the enzyme acetylcholinesterase [49]. Asphyxiants, also known as blood agents, are substances that cause tissue hypoxia [49]. Choking or pulmonary agents are the general class of gases that are toxic to the human lung when inhaled [49].

Although the U.S. did not use chemical weapons during World War II, quantities of chemical weapons were produced and deployed to Europe for use in case Germany initiated chemical warfare [50]. After the war, thousands of American soldiers were exposed to warfare agents during Cold War programs or in accidents

[51]. From 1967 to 1970, the U.S. disposed of chemical weapons by sinking ships laden with the weapons in the deep Atlantic Ocean. In the 1973 - 1976, nearly 4,200 tons of nerve agents were destroyed by chemical neutralization and incineration at Tooele Army Depot and Rocky Mountain Arsenal [52]. In the 1980s, the U.S. began stockpile reductions; and Public Law 99-145 was enacted, requiring the safe destruction of the U.S. military chemical weapons stockpile [52]. In 1993, the U.S. signed the Chemical Weapons Conventions (CWC), which required the destruction of all chemical weapon agents, dispersal systems, and chemical weapons production facilities: (1) to destroy 1 % of chemical weapons by April 2000; (2) to destroy 20 % of CW agents by April 2002; (3) to destroy 45 % of CW agents by April 2004; (4) to destroy 100 % of CW agents by April 2012. By 2007, the U.S. met the first three objectives. However, only 90 % of chemical weapons destruction in the U.S was verified by OPCW (Organization for the Prohibition of Chemical Weapons) by 2012 [53].

3.4 Chemical and Biological Warfare Protection

Though most nations in the world had signed and ratified the CWC and chemical weapons will ultimately become something that only exist in the world's history books, chemical weapons still threaten people's lives, especially those in the military. It is extremely important to develop protective equipment against chemical warfare agents. The United States Military has some of the most technically

advanced field equipment in the world to protect against CBW agent including respirators and protective garments.

Respirators. A gas mask is a mask put on over the human face to protect the wearer from inhaling CBW agent, especially toxic gas. It has been used in both World War I and World War II to protect soldiers from gas attacks. In 1847, Haslett invented the modern gas mask that only filtered dust from the air [54]. The first use of toxic gas as a CW agent was in 1915. In the same year, American inventor James Bert Garner invented a gas mask that contained activated charcoal to adsorb the hazardous gas [55]. Later, the US Army Chemical Warfare Service developed the gas mask that people in the USA are familiar with today [56].

Protective Garment. For body protection, several types of NBC (Nuclear, Biological, Chemical) protective clothing were developed against CBW agents. They are either permeable or impermeable.

1) Impermeable Garment

In 1989, impermeable protective suits were developed for defense personnel who had a large chance to contact CBW agents while performing their tasks [60]. The impermeable NBC-protective suit provided five hours of protection against sulphur mustard (HD) and sarin (GB). To wear the suit, two persons are required to help the person donn or doff the garment, which is very inconvenient in case of an emergency. The huge heat load of the impermeable protective garment creates an

intolerable barrier against the normal cooling processes of the human body, and reduces the wear time before heat exhaustion.

2) Permeable Suits

To relieve the heat stress in NBC-protective clothing, a permeable suit was developed [3]. The suit was made of a porous material containing activated charcoal which was able to absorb the CW agents while allowing air to flow through the porous structure. Many disadvantages are associated with this porous material including aerosols penetration, low durability, and easily contamination by organic compounds such as fuels, oils or poisons. Hence, some other materials were used to produce selective water permeable clothing [3]. It was made of hydrophilic plastic materials such as poly vinyl alcohols, polyurethanes, and cellophane. However, these water permeable polymers are not good barriers against CWA when they are wet.

Later, Saratoga carbon pellet technology developed by Blucher GmbH gained much attention among the forces of USA [57]. The Saratoga contained spherical activated carbon adsorbers that provide great chemical agent adsorption, comfort, launderability, and reusability. The adsorbing capability for a full range of hazardous CW agent makes the Saratoga carbon pellet protective clothing effective. An improved CWU/66P CW protective clothing system was then developed for the US aircrew, which exhibited good chemical agent protection capability before and after repeated washings, reduced thermal burden on the individual, was reusable,

and provided durability for long term use [58]. Now the activated carbon is still used in all the permeable chemical protective clothing made for defense personnel [59].

Another active carbon protective textile, the Saratoga system, is a family of different materials using spherical activated carbon adsorbers that have demonstrated excellent chemical agent protection, comfort, launderability and reusability [59]. Polybenzimidazole (PBI) Saratoga Protective textile was made by first bonding small spherical adsorbers to the outer shell fabric made from PBI and Nomex blend. After numerous physical, chemical, and physiological laboratory tests, the new personal chemical protective suit of the U.S. military services was developed by Blucher GmbH [60]. Later, the Saratoga chemical protective overgarment of the U.S. Marine Corps was established as benchmark [59]. The following are kept as requirement for a chemical protective suit (a) wear time in the non-chemical environment for more than 45 days; (b) protection time for more than 24 hours; (c) 6 times of field launderability; (d) overgarment, aviator and duty uniform as suit configurations and; (e) seven sizes ranging from small to large.

Triethylene diamine (TEDA) carbon (a chromium-free carbon) developed by Dharcoal [61] was impregnated with metal oxides such as Ag, Cu, Zn, and Mo in the presence of TEDA. It is used in the existing facemask and the protective clothing. NBC filters with TEDA carbon provide a high level of protection against all chemical warfare with only a few exceptions. The mechanisms for TEDA carbon filters are

physical adsorption, generally followed by agent decomposition effected by metal oxide impregnates.

3) Prospective NBC Protective Materials

NBC protective clothing currently used against CBW agents contain activated charcoal impregnated with metal ions, which physically adsorb nerve and blister agents thereby creating disposal hazards after its usage. Nanotechnology has been researched in various aspects as well as in catalysis. Metal oxide nanoparticles (MONPs) such as ZnO, TiO_2, Al_2O_3, and MgO are potential catalysts for the decontamination of CBW agents because they possess unique properties such as high surface area, great amount of highly reactive edge and corner defects, shapes, and large porosities [62]. They have been shown to be highly efficient and active adsorbents for many toxic chemicals including air pollutants, CW agents, acidic gases, and pesticides. Destructive adsorption occurs on the surface of the nanoparticles; therefore toxics can be transformed to less toxic compounds [63].

3.5 Organophosphorus Compounds

Organophosphorus compounds are organic compounds containing carbon-phosphorus bonds or they are organic derivatives of inorganic phosphorus acids. Phosphorus (V) and phosphorus (III) are two predominant categories of organophosphorus compounds, which are classified by the oxidation states of phosphorus [64]. Organophosphorus compounds have been used for a wide variety

of applications such as therapeutic agents, agricultural chemicals, plasticizers, lubricants, flame-retardants, fuel additives, and, most notoriously, as chemical warfare agents. Some organophosphorus compounds such as nerve agents are included in the most toxic substances ever created by man, which are lethal to humans at minuscule doses [64].

3.5.1 Organophosphorus compounds as nerve agents

Many organophosphorus compounds are potent nerve agents. Nerve agents are organophosphorus compounds that are capable of inhibiting the enzyme acetylcholinesterase [65]. These compounds are categorized as G (Germany) series agents: GB (sarin), GD (soman), GA (tabun), GF and V (venomous) series agents: VE, VG, VM and VX [65]. The G series of weapons were developed by the Nazi government in the 1930s. In the early 1950s, the British produced VX nerve agent, which was much more potent than the G series [66]. Fig. 2.1 shows the chemical structure of sarin and VX agent [65].

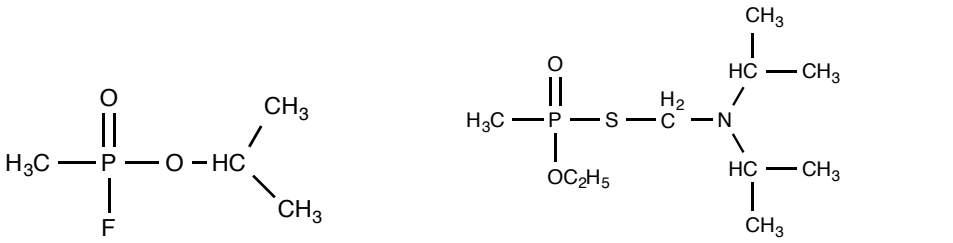

Sarin (GB)
2-(fluoro-
methylphosphoryl)oxypropane

VX
O-ethyl S-[2-(diisopropylamino)ethyl]
methylphosphonothioate

Figure 2.1 Chemical structure of sarin and VX agent

3.5.2 Organophosphate Poisoning

Nerve agents have the same mechanism of action as organophosphate pesticides. Toxicity is due to the inhibition of the enzyme acetylcholinesterase (AChE) in the nervous system and at the motor end-plate. AChE normally functions to degrades acetylcholine in the synapse. Thus, inhibition of AChE allows accumulation of acetylcholine with subsequent excessive stimulation of acetylcholine receptors. Though some degree of AChE inhibition can be tolerated, more extensive inhibition (>50-60%) of AChE may cause muscle fasciculation, involuntary movements, and eventually respiratory depression [66]. Organophosphorus pesticides as well as nerve agents can be absorbed by all routes, including inhalation, ingestion, and dermal absorption [67].

3.6 Methyl Parathion

Methyl parathion (MP) as shown in Fig. 2.1, also known as parathion methyl, O,O-dimethyl O-4-nitrophenyl phosphorothioate, was one of the most widely used OP insecticide in the United States [67]. The structure of VX agent is very similar to methyl parathion, and they have the same mechanism of toxicity. Therefore, methyl parathion can be used as a simulant for VX agent.

3.6.1 Photocatalytic degradation of methyl parathion

As an efficient degradation method, photocatalytic degradation of methyl parathion has been previous investigated [68, 69, 70]. Oxidation [68, 69],

isomerization [69] and hydrolysis [70] are three mechanisms that may occur in the photocatalytic degradation of methyl parathion. Scheme 3.1 shows the possible photocatalytic decontamination of methyl parathion pathway.

3.6.1.1 Oxidation

Most of the previous studies indicated that the first step of degradation was dominated by oxidation. Moctezuma et al. [68] proposed a reaction mechanism for the photocatalytic oxidation of methyl parathion (Scheme 3.1). They concluded that MP is first oxidized to methyl paraoxon (MPO) with MPO being oxidized later to 4-nitrophenol. 4-nitrophenol then reacts with $HO\cdot$ radicals and is converted to hydroquinone. At the same time, NO_2^- produced was oxidized to the more stable nitrate anions, NO_3^-. PO_4^{3-} were also observed, which supports Step 3b that of the decomposition of dimethyl phosphoric acid.

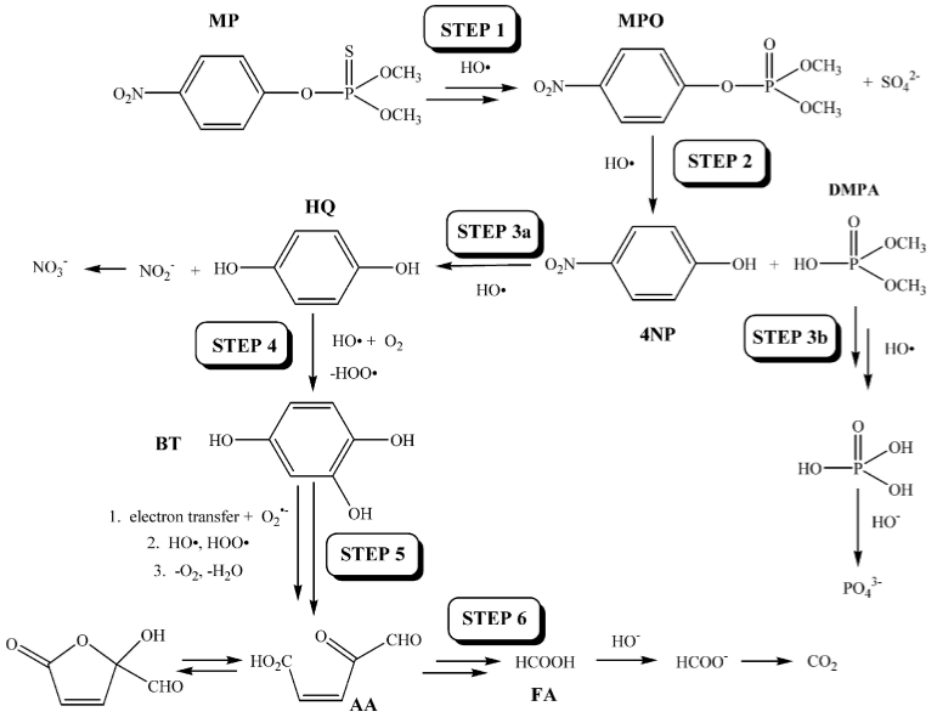

Scheme 3.1 Proposed mechanisms for the photocatalytic oxidation of methyl parathion. MP: methyl parathion; MPO: methyl paraoxon; 4NP: 4-nitro phenol; HQ: hydroquinone; BT: 1,2,4-benzenetriol; AA: aliphatic acid; FA: formic acid [68]

Evgenidou et al. [69] developed a similar mechanism for photocatalytic oxidation of methyl parathion. As shown in Scheme 3.2, they proposed 8 compounds as intermediate degradation products. Oxidation attack of the · OH on the P=S bond occurred first, resulting in the formation of methyl paraoxon (compound 6). The continuous attack of · OH followed by the rupture of P–O bond resulted in the formation of the 4-nitrophenol (compound 5) and dialkylphosphates (compounds 1–4).

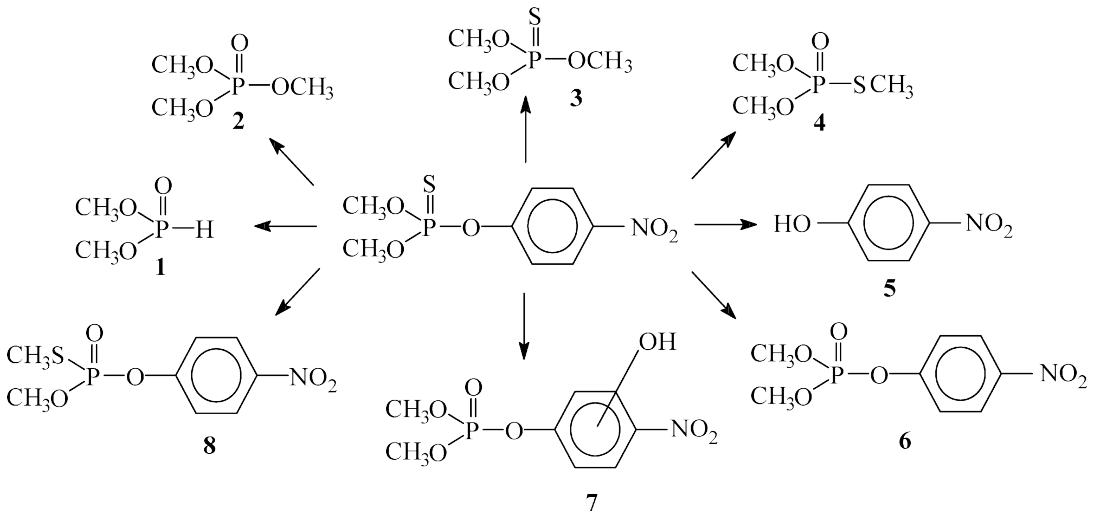

Scheme 3.2 Photocatalytic degradation scheme of methyl parathion in TiO_2 suspensions. [69]

3.6.1.2 Isomerization

Isomerization also has been shown to occur as an initial step in degradation as shown in Scheme 3.2 [69]. Mass spectrometry was used to prove this result. Compound 7 was attributed as the ring-hydroxylated derivative of methyl parathion. It exhibits the same characteristic ions with methyl parathion and its molecular ion M+ at m/z 279 correspond to the addition of –OH group to the phenyl ring. Compound 8 was identified as the S-isomer of methyl parathion. Its spectrum has common features with that of methyl parathion with slightly stronger M+ intensity, more abundant m/z 125-fragment ion, and weaker intensities than for the rest of the common ions.

3.6.1.3 Hydrolysis

Less has been published about methyl parathion degradation by hydrolysis. Seger and Maciel [70] investigated different phosphorus environment using ^{31}P NMR. They mentioned that hydrolysis of methyl parathion can also happened in the first step of methyl parathion degradation. Hydrolysis of methyl parathion can result in either removal of the 4-nitrophenoxy groups or a methoxy group.

Although few researches were focused on the hydrolysis decontamination of methyl parathion by photocatalysis, there are some studies on similar topics. Yang et al. [72] found that VX undergoes hydrolytic degradation over time with the presence of small amount of water (6%). However, the complete decontamination time was over 800 hours. Recently, Alvim et al. [73] proposed a reaction mechanism for the degradation of O,S-dimethyl methylphosphonothioate (DMPT), a VX-like organophosphorus compound, catalyzed by the MgO surface. With the presence of water, DMPT was either decomposed to $HOPO(CH_3)(SCH_3)$ and $HOCH_3$, or to $HOPO(CH_3)(OCH_3)$ and $HSCH_3$. It is noticed that both studies discussed that domination by hydrolysis decontamination requires the presence of water. According to the book “The Detoxification and Natural Degradation of Chemical Warfare Agents” by Ralf Trapp [5], the hydrolysis of VX agent depend significantly on the contact surface between the aqueous and the organic phase.

3.7 Analytical Methods

To investigate the tentative decontamination, the hypothesized mineralization pathway, the decontamination efficiency, and the reusability of photocatalysis, various equipment and theoretical deduction methods were employed.

3.7.1 Phosphorus-31 NMR Spectroscopy

As an analytical technique, phosphorus-31 NMR spectroscopy (^{31}P-NMR) is very frequently used to assay purity and to assign structures of phosphorus-containing compounds because their signals are mostly well resolved and occur at characteristic frequencies. ^{31}P has an isotopic abundance of 100% and a relatively high magnetogyric ratio, and its nucleus also has a spin of ½, which makes spectra relatively easy to interpret. In the area of organophosphorus chemistry, ^{31}P-NMR was largely employed due to its ability to differentiate organophosphorus with varies structure around the phosphorus [65].

In the study conducted by Seger and Maciel [70], predicted degradation products from hydrolysis, isomerization, and oxidation and the solid-state data ^{31}P chemical shifts obtained from various literature sources were listed. They used this information to study the decomposition of methyl parathion sorbed on partially hydrated kaolin and montmorillonite clays. Topalov et al. [71] successfully used ^{31}P-NMR to follow the kinetics of the degradation fenitothion, an insecticide, into inorganic phosphorus.

3.8 High Performance Liquid Chromatography-Mass Spectroscopy/Diode Array UV-vis Detector (LC-MS/DAD)

High performance liquid chromatography (HPLC) is a technique used to separate the components in a liquid mixture, therefore to identify each component, and to quantify each component. LC-MS/DAD used in the current study is an analytical chemistry technique that combines the physical separation capabilities of HPLC with the mass analysis capabilities of mass spectrometry (MS) and the UV-vis absorption analysis capabilities of diode array detector (DAD). Because of its great analytical capability, LC-MS/DAD is very useful in many applications. In this study, it was used to identify and quantify the degradation product of methyl parathion.

3.8.1 High Performance Liquid Chromatography (HPLC)

There are two types of HPLC, normal phase HPLC and reversed phase HPLC. In normal phase chromatography, the stationary phase is hydrophilic silica and therefore has a strong affinity for hydrophilic molecules in the mobile phase. Thus, the hydrophilic molecules in the mobile phase tend to form attractions with the column, while the hydrophobic molecules pass through the column first. For reversed phase HPLC, the silica in the column is modified to be non-polar (hydrophobic) by attaching long hydrocarbon chains onto its surface [74]. A polar mobile phase is employed in reversed-phase chromatography. In this case, strong attraction is form between the polar mobile phase and the hydrophilic or polar molecules in the mixture. Therefore, polar molecules in the mobile phase pass

through the column faster with the movement of mobile phase. Non-polar molecules in the mixture move slower through the column for two reasons: (1) non-polar molecules in the mixture tend to form van der Waals forces with the hydrophobic stationary phase; (2) non-polar molecules are less soluble in the polar mobile phase and spend less time on the column as they are moving with the polar solution [74]. Most research, including the current study, use reversed phase HPLC.

The time taken for a particular compound to reach the detector is called retention time. For reversed phase HPLC, polar molecules in the mixture have shorter retention time than non-polar molecules [74]. In one liquid mixture, different compounds have different retention times. When standards of each compound are provided, the amount of each compound in the mixture can be calculated by comparing with a calibration curve. Retention time is also important evidence for qualitative determination.

3.8.2 Liquid Chromatography Mass Spectroscopy (LC-MS)

LC-MS is an analytical chemistry technique that combines separation capabilities of HPLC with the mass analysis capabilities of mass spectrometry [75]. LC-MS is a very powerful technique that has great sensitivity and selectivity. Unlike GC-MS, LC-MS is suitable for analyzing polar compounds, non-volatile samples, and thermally instable compounds. However, LC-MS is not as good for library matches of unknowns when in scan mode as GC-MS.

LC-MS is also a very useful in analyzing organophosphate pesticides and their

degradation products. In a study by Aguilar et al. [76], important positive-ion and negative-ion mass spectra fragments and their relative abundances for some organophosphate pesticides, includes parathion-ethyl, obtained from LC-MS were listed. Significant fragmentation was observed for parathion-ethyl due to loss of NO • in positive-ion mass spectra, losses of $O=P(OCH_3)_2$ or $S=P(OCH_3)_2$ in negative-ion mass spectra. Lacorte et al. [77] indicated that the fragment peak for $[(CH_3O)_2P(OH)]^+$ was most abundant for methyl parathion. For fenthion, another organophosphorous pesticide, and its degradation products, group-specific fragments like $[(CH_3O)_2PO_2]^+$, $[(CH_3O)_2PO]^+$, and $[(CH_3O)_2PS]^+$ at m/z 125, 109, and 125, were observed [78].

3.8.3 Photodiode Array UV-vis Detector (DAD)

A photodiode array detector (DAD) can be used to obtain complete UV adsorption spectra for the HPLC peaks. Since the ability of an organic compound to absorb UV radiation is dependent on its electronic structure, UV spectra can be used as a way to characterize unknown organic compounds [79]. When a compound contains chromophores, groups of atoms responsible for UV absorption of the molecule, it can be detected and characterized by DAD, therefore identifying the unknown compound. For many electronic structures, the absorption does not occur in the ultraviolet region. In practice, only those compounds contains conjugated systems (chromophores) have UV absorption, and only few peaks can be detected by UV-vis detectors, which makes the UV spectra too simple to do qualitative

analysis. However, it is very easy to differentiate the compounds with or without a certain kinds of chromophores.

3.9 Octanol-Water Partition Coefficient

One of the goals of the current research is to predict the photocatalytic degradation pathway for methyl parathion in aqueous-ethanol solvent. To more accurately predict it, degradation intermediates in the sample after reaction need to be identified, which means, each unknown compound separated in the HPLC column needs to be analyzed. Octanol-water partition constants are used to predict the HPLC retention time of some candidates for unknown compounds in a mixture.

Octanol-water partition coefficient (K_{ow}) is defined simply by;

$$K_{ow} = \frac{C_{octanol}}{C_{water}} \tag{11}$$

where $C_{octanol}$ is the molar concentration of the organic compound in the octanol phase and C_{water} is the molar concentration of the organic compound in water when the system is at equilibrium [80].

K_{ow} can be calculated based on structural group contributions by;

$$\log K_{ow} = \sum f_i + \sum F_j \tag{12}$$

where f_i values quantify contributions from each structural unit and F_j values account for special intramolecular interactions [80].

Another method to estimate the K_{ow} uses HPLC. In reverse phase HPLC, the

solute is transported in a polar mobile phase through a nonpolar stationary phase. As the organic solutes move through the system, they partition between the polar mobile phase and the non-polar stationary phase. For a series of structurally related compounds of similar size and shape, there is a good correlation between K_{ow} and retention time, especially for HPLC using C_{18} stationary phase [80]. To account for operational differences in HPLC, the capacity factor was actually used instead of retention time. The capacity factor (k) is the retention time of a compound relative to a non-retained chemical species. By creating the linear regression model between Log K_{ow} and Log t, it is very easy to predict K_{ow} value if retention time is known. In this thesis, K_{ow} was calculated based on the chemical structure and the linear regression model was used to predict the retention time of candidates for degradation intermediates. Although few researchers used K_{ow} to predict and compare the retention time, and thus to identify each compound in HPLC, K_{ow} can be used as a tool to differentiate each peak in HPLC chromatograms since there is a good correlation between K_{ow} and retention time.

3.10 Hansen Solubility Parameters

Hansen solubility parameters were used as a tool to select a proper solvent for photocatalytic degradation reaction. There are two requirements for a proper solvent: (1) solubility of methyl parathion and its tentative degradation products; (2) low toxicity.

Hansen solubility parameters are a way of predicting if one material will

dissolve in another forming a solution. Each molecule is characterized by three Hansen solubility parameters, δ_d, δ_p, and δ_h, which are energy from dispersion forces, intermolecular forces, and hydrogen bonds between molecules. These three parameters for a certain compound can be estimated from molecular structural contributions by:

$$\delta_d = (\sum_z {}^zF_d) / V \tag{13}$$

$$\delta_p = (\sum_z {}^zF_p{}^2)^{1/2} / V \tag{14}$$

$$\delta_h = (-\sum_z {}^zF_h / V)^{1/2} \tag{15}$$

where ${}^zF_d$ and ${}^zF_p$ represent the dispersion and polar group molar attraction contributions, and ${}^zF_h$ represents the hydrogen bonding parameter group contributions. V is the molar volume for the molecule. Values of ${}^zF_d$, ${}^zF_p$, and ${}^zF_h$ for some group are provided in the CRC Handbook [83].

This method has several limitations: (1) the values reported by different authors of particular group contributions show considerable variation; (2) some numbers of group contributions for some common groups are missing; (3) only first-order groups were included in this method; (4) the correlation between estimated and experimental values of Hansen solubility parameters were not provided, thus the accuracy of the prediction is unknown. In 2008, Stefanis et al. [82] established a new group contribution method for Hansen solubility parameters prediction. In this method, the molecular structure of each organic compound can be

described using two kinds of functional groups: first-order groups (UNIFAC groups) that describe the basic molecular structure of compounds and second-order groups that are based on the conjugation theory. The second-order groups give a physical meaning to the method, which improves the accuracy of predictions significantly, and this is an advantage compared to other group-contribution methods.

The equation for the estimation of δ_d, δ_p, and δ_h, are the following:

$$\delta_d = \sum_i n_i F_{di} + W \sum_j m_j S_{dj} + 17.3231 \quad (16)$$

$$\delta_p = \sum_i n_i F_{pi} + W \sum_j m_j S_{pj} + 7.3548 \quad (17)$$

$$\delta_h = \sum_i n_i F_{hi} + W \sum_j m_j S_{hj} + 7.9793 \quad (18)$$

Where F_i is the contribution of the first-order group of type i that appears n_i times in the compound, and S_j is the contribution of the second-order group of type j that appears m_j times in the compound. The constant W is equal to 0 for compounds without second-order groups and equal to 1 for compounds that have second-order groups. Values of F_i and S_j for each group were provided in a paper by Stefanis'and Panayiotou [82].

These three parameters can be treated in three dimensions, also known as Hansen space. The nearer two molecules are in the Hansen space, the more likely they are to dissolve into each other. To calculate the distance between Hansen parameters in Hansen space, the following equation was used:

$$R = [(\delta_{d1} - \delta_{d2})^2 + (\delta_{p1} - \delta_{p2})^2 + (\delta_{h1} - \delta_{h2})^2]^{1/2} \quad (19)$$

In the current research, solubility parameters were also used as a supplementary data for identification of the decontamination intermediates since relative retention time of the compounds separated in reversed phase HPLC are related to the solubility parameter. Although the calculated solubility parameters were not able to accurately infer the retention time of each tentative compound, hydrophobic compounds come out later than hydrophilic compounds on a reversed-phase column in HPLC [74].

4. Experimental

4.1 Materials

Polyacrylonitrile (CAS 2504-41-9) was acquired from Sigma-Aldrich (St. Louis, MO). It had a weight average molecular weight of 150,000, a glass transition temperature of 85.0°C, a melt temperature of 317°C, a density of 1.184 g/mL at 25°C, a refractive index of 1.514, and a chemical formula of C_3H_3N. PAN was chosen over other polymers because it is inexpensive and easy to electrospin.

Zinc oxide powders with two different particle sizes (<5 μm and <50 nm) were also acquired from Sigma-Aldrich. ZnO with particle size < 50 nm were used to produce nanofibers, it had an surface area over 10.8 m^2/g. ZnO with particle size < 5 μm were used to verify the photocatalytic degradation activity of ZnO on methyl parathion.

The organophosphate pesticide chosen for this research was methyl parathion that has been used as a simulant for more harmful organophosphates, VX agent, etc. Methyl parathion was purchased from Supelco Analytical (Bellefonte, PA), its chemical name is O,O-dimethyl O-(4-nitrophenyl) phosphorothioate, the molecular weight is 263.21 g/mol, and the chemical formula is $C_8H_{10}NO_5PS$. The degradation products of methyl parathion, methyl paraoxon and 4-nitrophenol were also purchased from Supelco Analytical; O,O,O-trimethyl phosphorothioate (OOO) was

purchased from Chem Service Incorporated (West Chester, PA); dimethyl phosphate, 1,2,4-benzenetriol and hydroquinone were purchased from Sigma-Aldrich.

Ethanol was purchased from Koptec (King of Prussia, PA); acetonitrile (HPLC grade) was purchased from Fisher Scientific (Fair Lawn, New Jersey); and N, N-dimethylformamide (DMF) was purchased from Malinckrodt Chemicals (Phillipsburg, NJ). Titan2 nylon syringe filters with a 0.45 μm pore size were from Thermo Fisher Scientific Inc. (Waltham, MA), and 5 mL syringes with Luer-Lok Tips were from BD Biosciences (Franklin Lakes, NJ). Polypropylene Membrane Filters with 47 mm diameters and 0.2 μm pore size were purchased from Sterlitech Corp. (Kent, WA).

4.2 Solvent Selection

The solvent system in this experiment was selected based on Hansen solubility parameters. Hansen parameters δ_d, δ_p, and δ_h of MP and its major degradation intermediates were estimated from molecular structural contributions by equations (16)-(18), Hexane, ethanol and water were selected as candidate solvents. Hansen parameters δ_d, δ_p, and δ_h for them were provided in CRC Handbook [74]. The distance of MP degradation products with hexane, ethanol and water were calculated using equation (19) to find out a proper solvent system.

4.3 Decontamination of Methyl Parathion with ZnO Nanoparticles

UV or near-UV photons initiate photocatalytic reaction. The equipment used in this study is a UV chamber (Fig. 4.1) produced by Rayonet (Model RMR-600) with 8 lamps with 4 watt and 3 in. tall, and the maximum wavelength of the UV light is 350 nm. To verify if methyl parathion reactivity follows photocatalytic mechanism, samples were prepared in either dark or UV. To investigate the methyl parathion degradation reaction with time, samples were reacted for different times. Each sample had 20 mL of the same 1.25 mg amount of methyl parathion in 4:1 v/v ethanol/water. Samples with or without 20 mg ZnO nanoparticles (<5 μm) were reacted for 6 hours in UV chamber or in the dark, resulting in 4 different treatments with four replicates each. After 1, 2, 3, 4, 5, and 6 hour, 1 mL of the solution in each sample was taken with a syringe and filtered by attaching a syringe filter, then transferred to an HPLC vial. Each sample was then run on the HPLC-DAD/MS.

a

b

Figure 4.1 (a) UV chamber used in this study; (b) the top view of the inside of UV chamber showing eight UV lamps and the center stage used to mount samples.

4.4 ZnO Nanoparticles Rinsing and Reuse

1.25 mg of methyl parathion was dissolved in 20 mL 4:1 v/v ethanol/water with 20 mg suspended ZnO nanoparticles (<5 μm); 4 replicates were prepared. Samples were then put into the UV chamber for 2 hours. The mixed dispersion was then filtered by the vacuum filtration system shown in Figure 4.2. In the vacuum filtration system, a membrane with pore size of 0.2 μm was used to filter the solution for each sample. By vacuum filtering the mixed dispersions after reaction, ZnO nanoparticles were separated from the solution and remained on the filtration membrane (pore size = 0.2 μm) (A). The filtered solution of each sample was collected in a disposal plastic tube (B) that had been placed in the flask. 1 mL of the filtered solution in each sample was taken with a syringe and filtered again by

attaching a syringe filter, then transferred to a HPLC vial. Each sample was then run on the HPLC-DAD/MS. ZnO nanoparticles were then rinsed in the top chamber of the filtration device (Fig. 4.2 A). In the rinsing process, the tube was taken out, and the liquid waste was collected in the flask. Each ZnO nanoparticle sample was rinsed twice with ethanol and then carefully transferred to a new testing glass jar and vacuum dried overnight at room temperature. The above procedure was defined as one cycle of usage. This procedure was repeated for four cycles to test the reuse activity of ZnO nanoparticles.

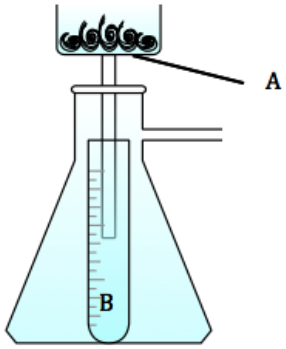

Figure 4.2 Vacuum filtration system; (A) filtration membrane with pore size of 0.2 μm; (B) disposal plastic tube to collect the filtrate

4.5 ZnO/PAN Nanofibers Preparation

To immobilize the ZnO particles, ZnO nanoparticles (<50nm) and polyacrylonitrile (PAN) were mixed in a 1:2 weight (0.25 g and 0.5 g) ratio at room temperature in 6.25 g N,N dimethylformamide (DMF) with stirring overnight to obtain a more homogeneous mixture for electrospinning. This mixture was placed in

a 5-mL syringe with a needle of 0.41 mm internal diameter. The nanofibers were generated by a syringe pump (PHD2000, Harvard Apparatus, Holliston, MA) with a 0.03 mL/min flow rate. The electric field was generated by a 20 kV electric charge. The distance from needle to collection was 15 cm. Scanning electron microscopy (SEM) (Leica 440, Leica Microsystems, Wetzlar, Germany) was used to characterize the ZnO/PAN nanofibers. The fiber diameter was estimated based on the SEM pictures using ImageJ software (National Institutes of Health. Bethesda, MD).

4.6 Decontamination of Methyl Parathion with ZnO Nanofibers

To determine the optimum degradation reaction time with ZnO/ PAN nanofibers, the following experiments were completed. Each sample contained 20 mL of the same 1.25 mg amount of methyl parathion in 4:1 ethanol/water solvent. Samples containing 200-mg nanofibers in 20 mL of methyl parathion solution were reacted in the UV chamber for one of seven times (2.5, 4, 6, 15, 27, 45, and 145 hour) with five replicates for each treatments. After the reaction time was complete, 1 mL of the solution was taken with a syringe and filtered by attaching a syringe filter, and then transferred to HPLC vial. Each sample was then run on the HPLC-DAD/MS. Methyl parathion standards were used to normalize for any drift of the HPLC instrument.

4.7 ZnO Nanofibers Rinsing and Reuse

To test the reusability of ZnO/PAN nanofibers, the filtration system in "ZnO Nanoparticles Refreshing and Reuse" (Section 4.4) was used in the following experiments. Each sample contains 1.25 mg of methyl parathion in ethanol/water solvent. Samples containing 200 mg of nanofibers in 20 mL of solution were reacted in the UV chamber for five days, with five replicates. After the reaction time was completed, 1 mL of the solution was taken with a syringe and filtered by attaching a syringe filter and then transferred to a HPLC vial. Each sample was then run on the HPLC-DAD/MS. The used nanofibers were separated by vacuum filtration as described in Section 4.4, then rinsed with ethanol and vacuum dried over night at room temperature. After rinsing with ethanol, the above decontamination and reuse procedure was then repeated six times, and samples run in HPLC-DAD/MS after each usage. Methyl parathion standards were used to normalize for any drift of the HPLC instrument.

4.8 HPLC-MS/DAD

For the determination of MP and intermediate organic compounds, samples were analyzed by high performance liquid chromatography (HPLC) combined with a diode array UV-vis detector (DAD) (Agilent HP1200, Santa Clara, CA). An Agilent XDB-C18 reversed phase column with 5-μm particle size, 4.6 × 159 mm dimension was used for separation of reactant and product intermediates at 25°C. The mobile phase was a mixture of 50:50 volume percent of acetonitrile and water with 1%

formic acid. The elute was delivered at a rate of 0.5 mL/min, and the runtime was 27 min. The wavelength of UV-vis detection was 280 and 320 nm. The mass spectrometer (MS) was a single-quadropole Agilent 6130 with a G1978B Multimode source that was set to scan for a mass-to charge ratio (m/z) from 20 to 550 m/z in both the positive and negative ES mode. The fragmentor was set at 120 in the positive mode and 80 in the negative mode. The mass detector spray-chamber parameters were set as follows: drying gas flow 6 L/min, nebulizer pressure 40 psig, drying gas temperature 300°C, vaporizer temperature 230°C, capillary voltage 2000 V, corona current in positive mode 4 μA, corona current in negative mode 5 μA, and charging voltage 2000 V.

Standards of 62.5 mg/L methyl parathion, 400 mg/L methyl paraoxon, 400 mg/L OOO, 400 mg/L 1,2,4-benzenetriol, 400 mg/L hydroquinone, and 70 mg/L 4-nitrophenol were run on the HPLC-MS-DAD to compare the degradation products found in the 4:1 v/v ethanol/water solutions. Methyl parathion standards (62.5 mg/L) were used to normalize for any drift of the HPLC instrument.

4.9 NMR Sample Preparation

To further investigate the degradation mechanism and the pathway, a more concentrated sample was examined by nuclear magnetic resonance (NMR), using liquid-state ^{31}P NMR. Sample was prepared as follows: 10 mg of methyl parathion was dissolved in 25 mL of ethanol/water with 700 mg suspended ZnO nanoparticles (<5 μm) and reacted in UV chamber for 1.5 hours. A MP standard was prepared with

10 mg methyl parathion in 25 mL ethanol/water. The solution in the sample and in the standard were taken with a syringe and filtered by attaching a syringe filter and then transferred into a NMR tube with 1 mL D_2O. Samples were sent to Cornell University Department of Chemistry and Chemical Biology for liquid-state ^{31}P NMR test. 1 mL of each filtered solution was transferred to the HPLC vial, and analyzed by HPLC-MS/DAD.

4.10 Octanol-water Partition Coefficient

Octanol-water partition coefficients (K_{ow}) for methyl parathion and possible decontamination products were either calculated by Estimation Program Interface (EPI) Suite (Syracuse Research Corp., Syracuse, NY) or obtained from literature. The retention times of MP, MPO, HQ, BT, and phosphoric acid were used to create the model for K_{ow} and retention time. The capacity factors (k) for each of MP, MPO, HQ, BT, and phosphoric acid were calculated using equation (13). By plotting Log t and Log K_{ow} for those compounds in a two-dimensional figure, a linear regression model was created between Log t and Log K_{ow} to predict the retention time for all other possible decontamination products. The predicted retention time was then compared with the retention time of the unknown peaks of intermediates to limit the numbers of candidates.

4.11 Statistical Analysis

To better understand the degradation of methyl parathion, statistical analyses were performed using JMP 9.0.0 software (SAS Institute Inc., Cary, NC). Two-way analysis of variance (ANOVA) with post-hoc mean comparisons with Tukey correction was completed to analyze if significant differences exist between methyl parathion amount in the samples based on two nominal variables, which in "Decontamination of Methyl Parathion with ZnO Nanoparticles" experiment (Section 4.3) are reaction time (1, 2, 3, 4, 5, and 6 hour) and reaction condition (with ZnO under UV, with ZnO in dark, without ZnO under UV, and without ZnO in dark). One-way ANOVA was performed in "ZnO Nanoparticles Refreshing and Reuse" (Section 4.4) to test if there was significant differences in the MP amount in the samples after repeated use (1, 2, 3, 4 reuse cycles), in "Decontamination of Methyl Parathion with ZnO Nanofibers" (Section 4.6) to test if there was significant differences of MP amount in the samples after various reaction time (2.5, 4, 6, 15, 27, 45, and 145 hour), and in "ZnO Nanofibers Refreshing and Reuse" (Section 4.7) to test if there was significant differences of MP amount in the samples after various number of reuse cycles (1, 2, 3, 4, 5, and 6 cycles). These mean comparisons are discussed in the "Results and Discussion" section.

5. Result and Discussion

5.1 Solvent Selection

In order to select a solvent system that would solubilize methyl parathion and its degradation products, Hansen solubility parameters were calculated. Based on Scheme 3.1, MPO, 4NP, HQ, BT, AA and FA are potential degradation products. So, solubility parameters for these compounds and the interaction radius of solubility parameters between each compound with water (R_{water}), hexane (R_{hexane}) and ethanol ($R_{ethanol}$) were calculated (Table 5.1). All compounds have smaller $R_{ethanol}$ value than their R_{water} and R_{hexane} values, so ethanol is a better solvent than water and hexane for the methyl parathion decontamination system. For photocatalytic reaction, water or oxygen is required to generate HO•, the major radical species that contribute to degradation of toxic chemicals. In the current research, water was added into the solvent system along with ethanol at the volume rate 1:4 (water : ethanol). This solvent system was used throughout the experiments.

Table 5.1 Calculated Hansen solubility parameters and the distance between compounds with water (R_{water}), hexane (R_{hexane}) and ethanol ($R_{ethanol}$) in Hansen space

Type / Solvent	Chemical Structure	Hansen Solubility Parameters δ_d(MPa$^{1/2}$)	δ_p(MPa$^{1/2}$)	δ_h(MPa$^{1/2}$)
Water	H-O-H [72]	15.5	16.0	42.3
Hexane	CH_3-CH_2-CH_2-CH_2-CH_2-CH_3 [72]	14.9	0	0
Ethanol	CH_3-CH_2-OH [72]	15.8	8.8	19.4

Compound	Abbr.		δ_d(MPa$^{1/2}$)	δ_p(MPa$^{1/2}$)	δ_h(MPa$^{1/2}$)	Interaction Radius of Solubility R_{water}	R_{hexane}	$R_{ethanol}$
1,2,4-benzenetriol	BT	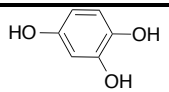	19.24	9.07	27.56	16.71	29.34	8.86
Hydroquinone	HQ	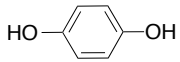	18.82	7.44	20.17	23.96	21.85	3.41
O,O,O-trimethyl phosphorothioate	OOO	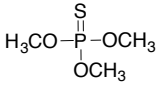	18.29	14.20	11.02	31.46	18.29	10.28
Methyl paraoxon	MPO	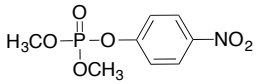	19.79	17.92	6.45	36.16	19.67	16.33
4- nitro phenol	4NP	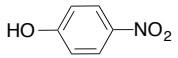	19.71	10.82	12.50	30.54	17.22	8.19
Methyl parathion	MP	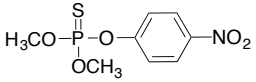	21.00	17.20	9.05	33.73	20.37	14.31

5.2 Decontamination of Methyl Parathion with ZnO Nanoparticles

In the experiments of reactivity of methyl parathion decontamination by ZnO nanoparticles in water/ethanol solvent, the amount of remaining MP in solution after different reaction time (1, 2, 3, 4, 5 or 6 hours) under various reaction conditions (under UV with ZnO nanoparticles, under UV without ZnO nanoparticles, in dark with ZnO nanoparticles, or in dark without ZnO nanoparticles) were measured by reversed phase HPLC. Chromatograms of methyl parathion sample after 0-6 hour reaction in UV chamber are shown in Figure 5.1. A calibration curve (Figure 5.2) was created using the MP standard samples with 0.3125 mg, 0.625 mg, 0.9375 mg, and 1.25 mg MP in 20 mL 4:1 v/v ethanol/water. The amount of MP in samples after reactions can be determined from the peak area of the detected MP and are reported in Table 5.2. A two-way ANOVA, followed by *post hoc* mean comparison with Tukey correction (α= 0.05, Q= 2.61), showed that the presence of ZnO (F ratio = 231.46, probability > F < 0.0001), the presence of UV light (F ratio = 261.76, probability > F < 0.0001), and the interaction between the presence of ZnO and the presence of UV light (F ratio = 224.32, probability > F < 0.0001) all had significant effects on the amount of methyl parathion remaining in the ethanol/water solution at the end of the reaction time. By running Tukey HSD (honestly significant difference) test for the interaction of the presence of UV and the presence of ZnO, MP amount remaining in the solution at the end of the reaction time under UV with ZnO was significantly

different from those under UV without ZnO (p-value < 0.0001), in the dark with ZnO (p-value < 0.0001), or in the dark without ZnO (p-value < 0.0001).

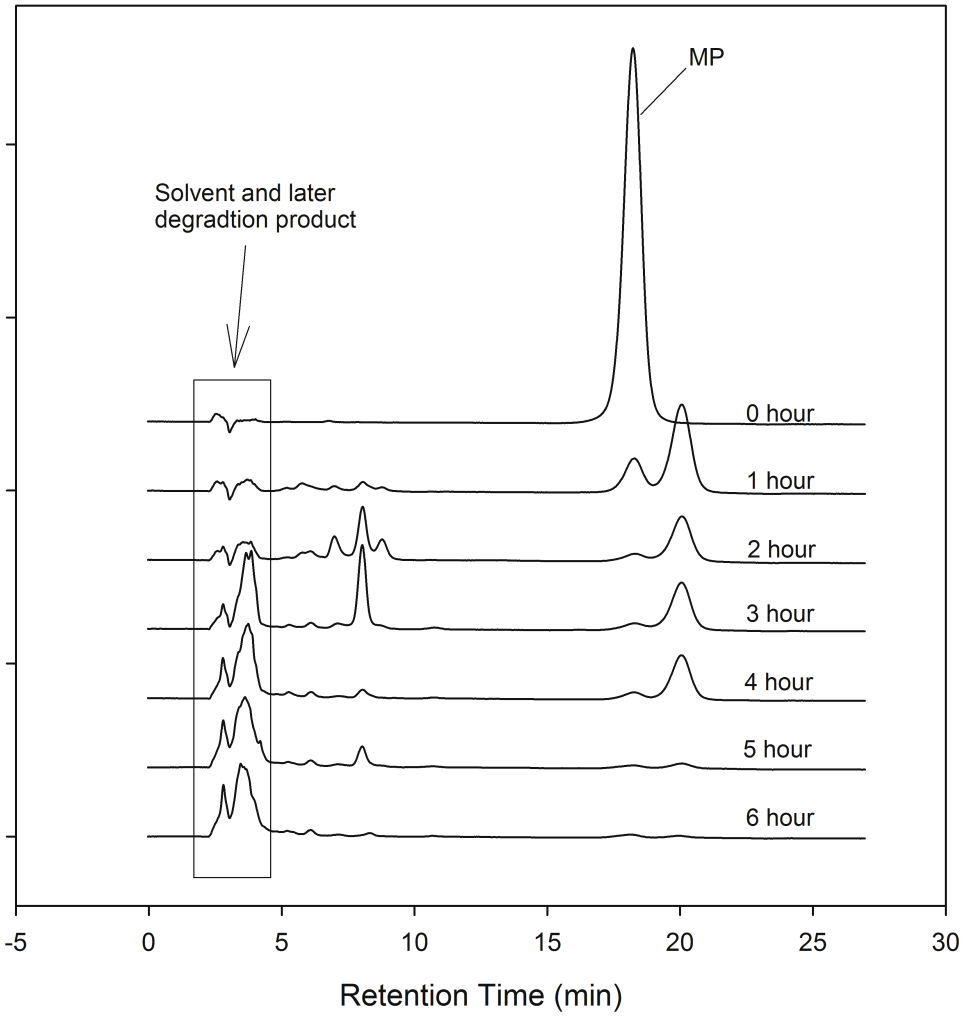

Figure 5.1. HPLC chromatograms of samples of methyl parathion solution after 0, 1, 2, 3, 4, 5, 6 hours in UV chamber with ZnO nanoparticles.

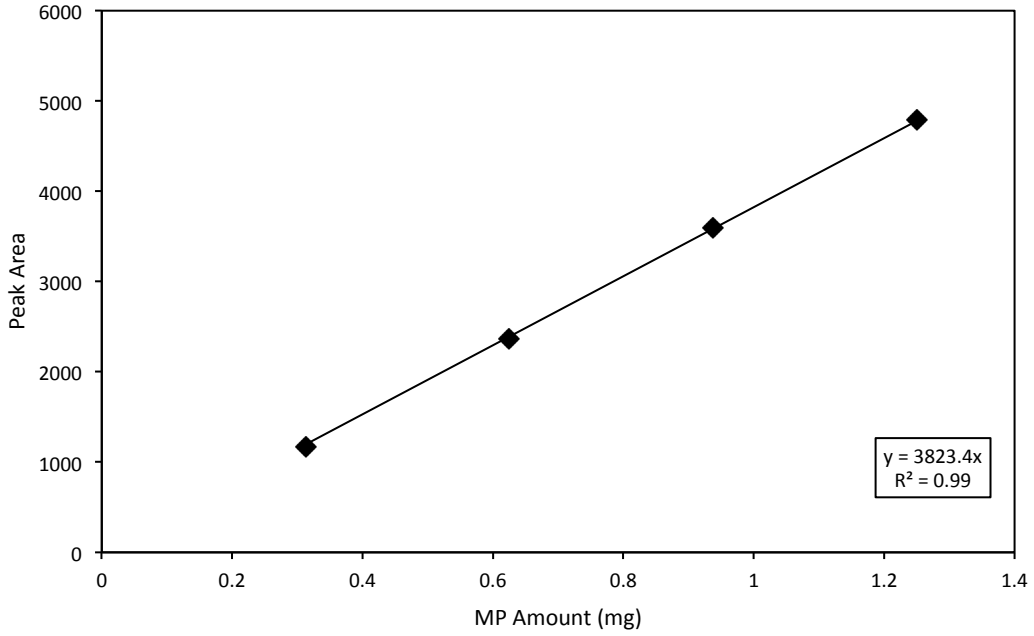

Figure 5.2 HPLC calibration curve of MP amount in 20 mL ethanol/water

Table 5.2 Methyl parathion amount in solution after degradation with ZnO nanoparticles based on reaction time and reaction condition of 1.25 mg

Reaction Condition	Reaction time (hour)					
	1	2	3	4	5	6
UV/with ZnO	0.20 (0.06)	0.02 (0.006)	0.02 (0.003)	0.02 (0.003)	0.01 (0.001)	0.01 (0.002)
Dark/with ZnO	1.24 (0.008)	1.24 (0.004)	1.24 (0.009)	1.24 (0.01)	1.24 (0.01)	1.24 (0.007)
UV/without ZnO	1.23 (<0.001)	1.21 (<0.001)	1.21 (<0.001)	1.21 (<0.001)	1.20 (<0.001)	1.19 (<0.001)
Dark/without ZnO	1.25 (<0.001)	1.25 (<0.001)	1.25 (<0.001)	1.25 (<0.001)	1.25 (<0.001)	1.25 (<0.001)

Reported values are average amount (mg) with their standard deviations in parentheses.

The methyl parathion amount decreased rapidly in one hour from 1.25 mg to 0.20 mg and then continued decreasing to 0.01 after six-hour reaction in samples reacted in UV chamber with ZnO. The amount of methyl parathion decreased little under the other three conditions, especially for those with no UV. For samples reacted under UV light without ZnO nanoparticles, methyl parathion amount decreased slowly. After six hours, the methyl parathion amount decreased from 1.25 to 1.19, which indicates that methyl parathion can be degraded under UV, but the rate was significantly lower than reactions in UV chamber with ZnO. In samples reacted in the dark with ZnO, methyl parathion amount was decreased by only 0.01 mg after one hour reaction with no further decrease within 6 hours. It is clear that the MP decontamination by ZnO is photocatalytic reaction activated by UV radiation.

Similarly, a calibration curve (Figure 5.3) for 4NP amount in 20 mL solution versus peak area was created using 4NP standards. By comparing the peak area with the calibration curve, the amount of 4NP in samples after 0-6 hour reaction in UV chamber was determined and reported in Figure 5.4. During photocatalytic degradation of methyl parathion, 4NP was created as a degradation product. The amount of 4NP slightly increased within 4 hours and decreased afterwards. Since the 4NP amounts detected in the experiments were very low (0.0019 mg), it is indicated that 4NP, a main intermediate compound, undergoes rapid degradation under UV with the presence of ZnO. The experimental result of this experiment demonstrate that under the reaction condition with UV and ZnO, the degradation rate for MP and intermediates species were both high.

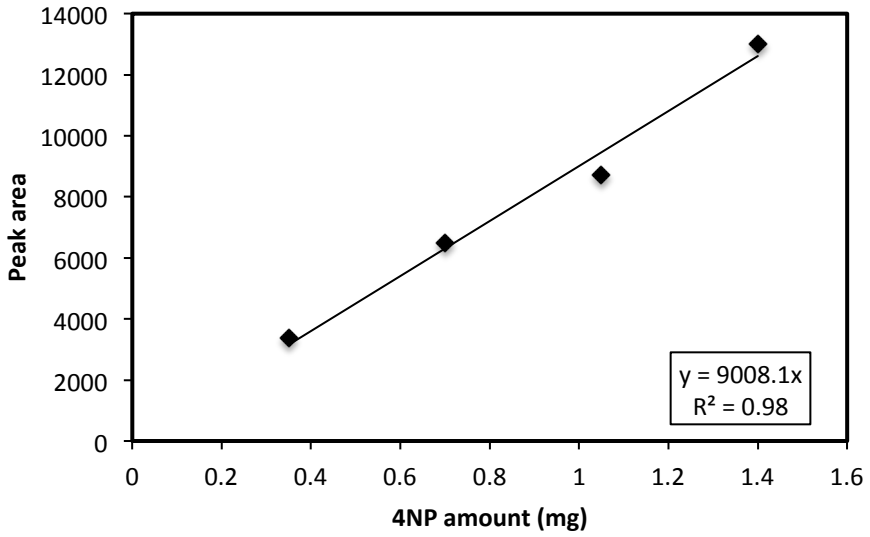

Figure 5.3 HPLC calibration curve of 4NP amount in 20 mL ethanol/water

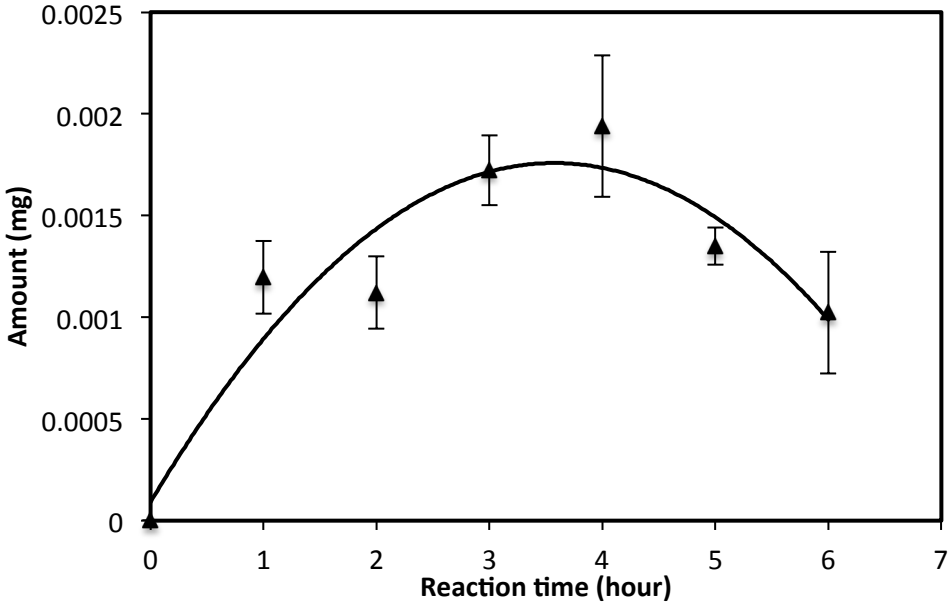

Figure 5.4 4-Nitrophenol amount and the trend line in solution after degradation with ZnO nanoparticles based on reaction time of 1.25 mg

5.3 Mechanism

As discussed in the Review of Literature (Section 3.6.1), hydrolysis, oxidation, and isomerization are three mechanisms that may occur in the photocatalytic degradation of methyl parathion. The possible first step of MP degradation under each mechanism is shown in Scheme 5.1. In the current thesis, the presence of water enhances the formation of HO•, which increased the rate of photocatalysis by hydrolysis. When using water and ethanol as the solvent there is little oxygen, which potentially eliminates the oxidation mechanism in these experiments. Thus, hydrolysis was hypothesized as the major mechanism for MP photocatalytic degradation with ZnO in a water and ethanol environment. In hydrolysis of MP, there are four possible mechanisms: (1) the O-aromatic ring bond was broke by HO•, and MP was degraded to 4-nitrophenol and O,O-dimethyl hydrogen phosphorothioate (Scheme 5.2); (2) one of the -OCH_3 group was reduced to –OH group by HO• (Scheme 5.3)); (3) an additional –OH group replaced one of the hydrogen attached on the aromatic ring and form the ring-hydroxylated derivative of MP (Scheme 5.4).

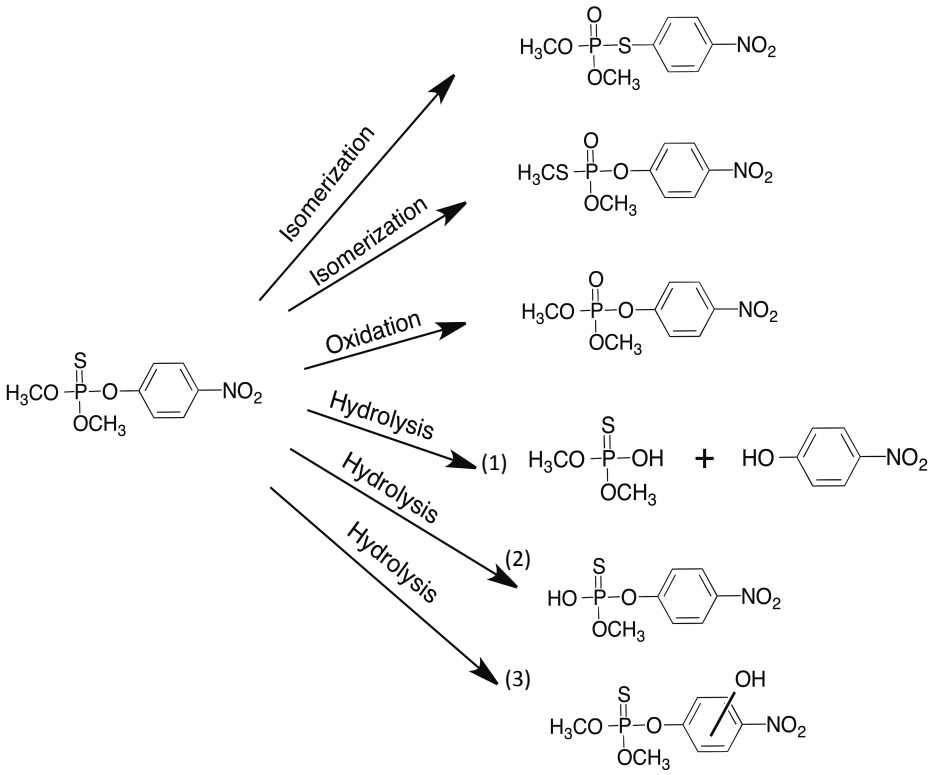

Scheme 5.1 Tentative photocatalytic degradation scheme of methyl parathion [69, 70, 71]

Based on the previous research on photocatalytic degradation of MP [69, 70, 71], proposed degradation pathway of MP hydrolysis (Scheme 5.2 - 5.4), oxidation (Scheme 5.5), and isomerization (Scheme 5.6) were considered. To confirm the hypothesis that hydrolysis is the major mechanism of MP photocatalytic decontamination in water/ethanol, HPLC chromatography, UV-vis spectrometry, mass spectrometry, ^{31}P NMR spectrometry and octanol-water partition coefficients were used to analyze and identify the degradation intermediates. Candidates for degradation intermediates were selected from Scheme 5.2 – 5.6. If the degradation intermediates are identified as species in hydrolysis degradation pathway (Scheme

5.2 - 5.4), it will be easy to conclude that hydrolysis is the major mechanism of photocatalytic decontamination in a water/ethanol solvent system.

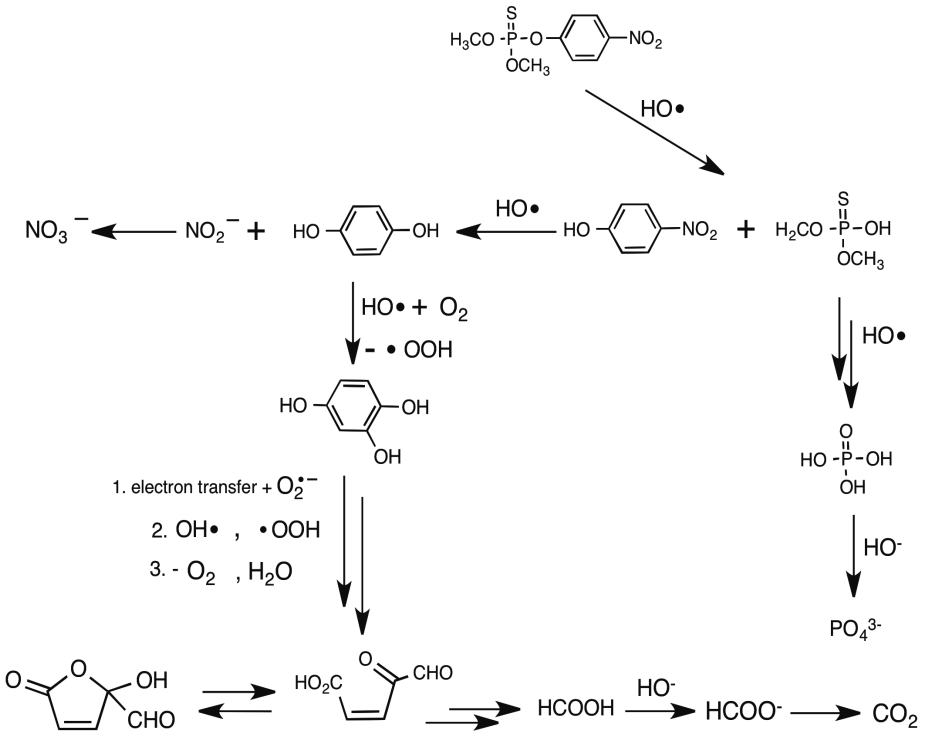

Scheme 5.2 Hypothesized overall decontamination mechanism for photocatalytic hydrolysis (1) of methyl parathion. [69, 71]

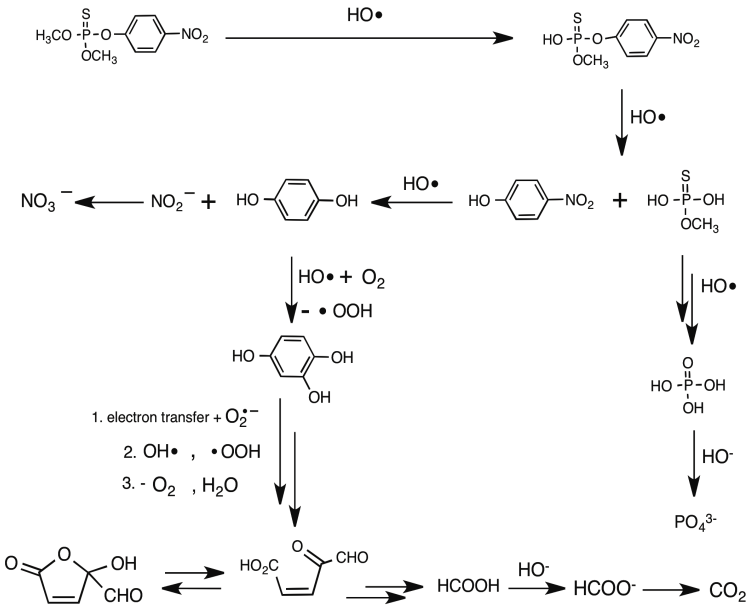

Scheme 5.3 Hypothesized overall decontamination mechanism for photocatalytic hydrolysis (2) of methyl parathion [69, 71]

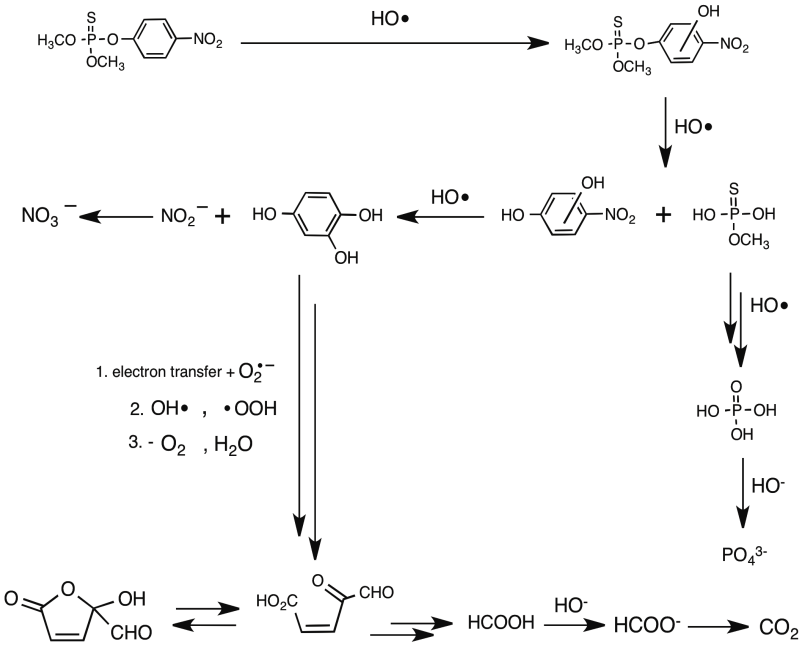

Scheme 5.4 Hypothesized overall decontamination mechanism for photocatalytic hydrolysis (3) of methyl parathion [68, 69]

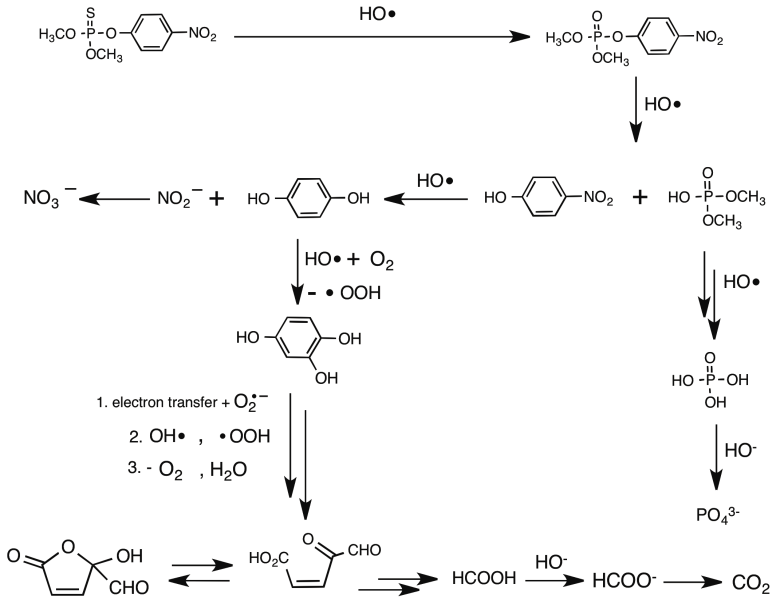

Scheme 5.5 Hypothesized overall decontamination mechanism for photocatalytic oxidation of methyl parathion [69]

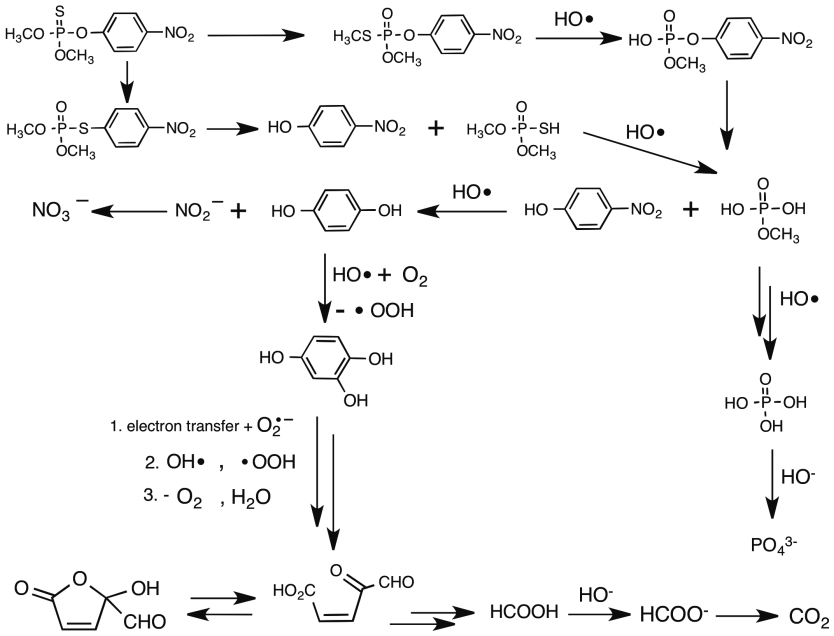

Scheme 5.6 Hypothesized overall decontamination mechanism for photocatalytic isomeration of methyl parathion [69, 71]

In Figure 5.1, the peak for methyl parathion was dramatically reduced for specimens after one-hour reaction, and several small peaks appeared. Those peaks are intermediates produced during photocatalytic degradation. With the increasing of reaction time, amounts of these degradation intermediates decreased and ultimately these intermediate products were mineralized.

The HPLC chromatogram for sample after 2-hour reaction is shown in Figure 5.5. As shown in Scheme 5.2 – 5.6, hydroquinone, 1,2,4-benzenetriol, and phosphorus acid are later degradation products reported in published research [70]. Through comparing the retention time of hydroquinone (3.36 min), 1,2,4-benzenetriol (2.84 min), and phosphorus acid (2.73 min) in Table 5.3, with new peaks in Figure 5.1 and Figure 5.5, peaks with retention time less than five minutes are possibly due to later degradation products. Other later degradation products, such as aliphatic acid and formic acid are more hydrophilic than HQ, BT, and phosphorus acid. As mentioned in Section 3.8.1, hydrophilic compounds have lower retention time in reversed-phase HPLC, thus the retention time of these later degradation products should be less than five minute, even they are not experimentally compared to standards in this thesis. Therefore, peaks in the rectangle frame in Figure 5.1 and 5.5 are thought to be later degradation products. In Figure 5.1, the height of these peaks increased with increasing reaction time, indicating the formation of hydrophilic compounds such as those expected as later degradation products (Scheme 5.2 - 5.6).

Table 5.3 Retention time detected from HPLC-DAD for the standard solution (A.) and unknown peaks (B.); methyl parathion (MP), methyl paraoxon (MPO), 4-nitrophenol (4NP), hydroquinone (HQ), 1,2,4-benzenetriol (BT), and phosphoric acid.

A. Standards

Type	Retention time (min)
Phosphoric Acid	2.73
BT	2.84
HQ	3.36
4NP	5.13
MPO	5.54
MP	18.32

B. Unknown peaks

#	Retention time (min)
a	5.21
b	6.24
c	7.00
d	8.03
e	8.89
f	18.16
g	20.07

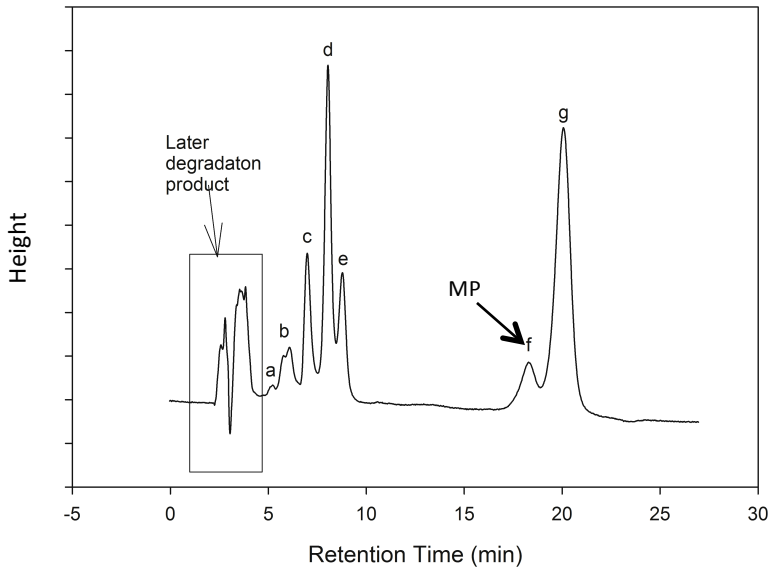

Figure 5.5 HPLC-DAD chromatogram of sample of methyl parathion solution after two-hour reaction. a, b, c, d, e, f and g are seven peaks that need identification.

Other than the later degradation products, peak f is identified as methyl parathion by comparing the retention time of MP standard. Peak a, peak b, peak c, peak d, peak e and peak g are unknown intermediates. By comparing the retention time of 4-nitrophenol (5.13 min) and methyl paraoxon (5.54 min) with the retention time of peak a (5.21 min) in Table 5.3, peak a was initially identified as 4-nitrophenol or methyl paraoxon. More analyzing on peak a is needed to determine whether it is 4NP or MPO.

Figure 5.6 shows the UV-vis spectrometry for unknown peaks (peak a, peak b, peak c, peak d, peak e, and peak g in Figure 5.3) obtained by HPLC-DAD. In UV-vis spectroscopy, UV absorption is high for compounds containing conjugated double bonds. In this specific situation of methyl parathion decontamination, the conjugated system is an aromatic ring. Since DAD has detected the UV-vis spectrometry of all unknown peaks, it is possible that peak a, b, c, d, e, f, and g all contain an aromatic ring.

As discussed in previous paragraph, peak a is identified as either 4NP or MPO. The UV-vis max absorption wavelength for peak a (Figure 5.6) is λ_{max} = 318 nm, while max absorption wavelength for 4NP and MPO standards are λ_{max} = 318 nm and λ_{max} = 275 nm. Since the max absorption wavelength for peak a was identical with that for 4NP, peak a was identified as 4NP. For the identification of other unknown peaks (peak b, peak c, peak d, and peak f in Figure 5.5), the result of octanol-water partition coefficients analysis and mass spectrometry analysis were used.

Peak a

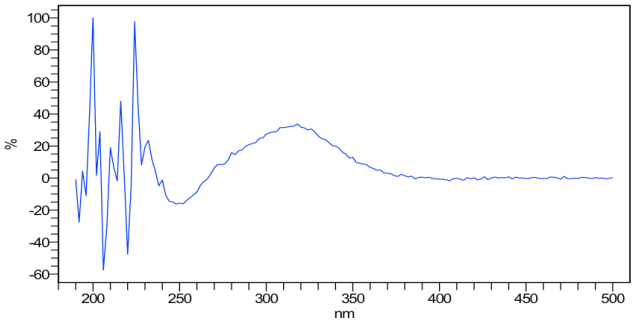

Peak b

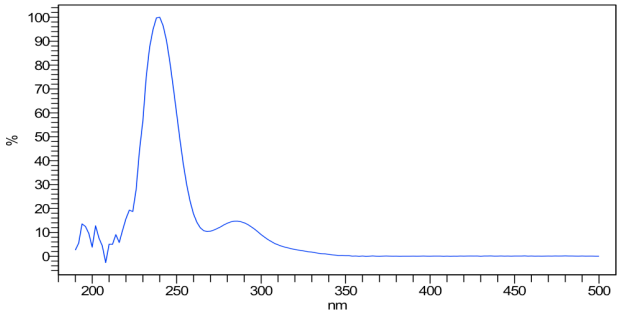

Peak c

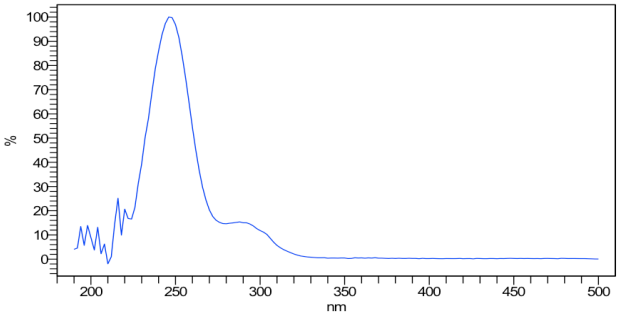

Peak d

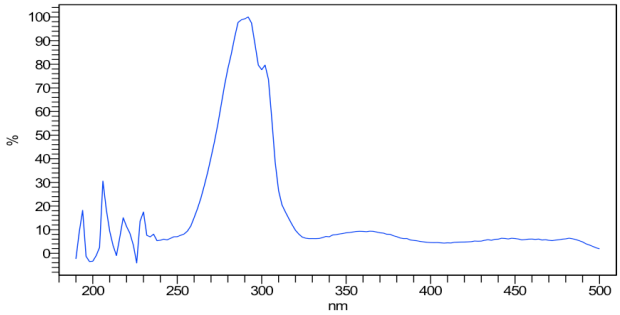

Peak e

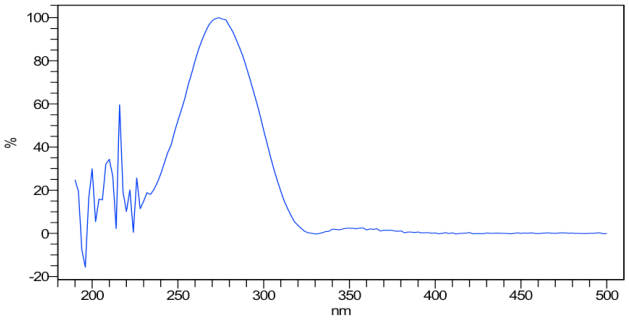

Peak f (MP)

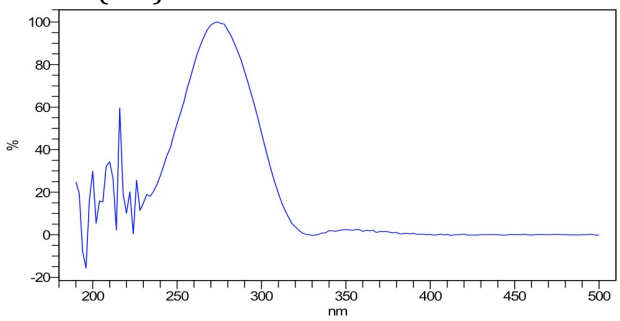

Peak g

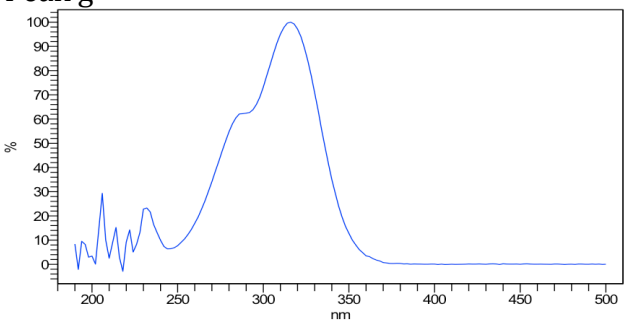

Figure 5.6 UV-vis figure for peak a, b, c, d, e, f, g. Peak labels correspond to those in Figure 5.5

Retention time for BT, MPO, MP, HQ and 4NP standards are reported in Table 5.3, and calculated Log K_{ow} values obtained by EPI Suite [84] of these compounds are reported in Table 5.4. As discussed in Review of Literature (Section 3.9), there is a high correlation between Log K_{ow} and Log t. Linear regression analysis on logarithmic retention times and logarithmic octanol-water partition coefficients of BT, MPO, MP, HQ and 4NP was used to create a model (Eq. 20) to predict the retention times for all the potential decontamination intermediates based on Schemes 5.2 – 5.6. The regression model was significant with $R^2 = 0.79$:

$$\log K_{ow} = 1.0194 \times \log t - 0.2489 \tag{20}$$

where K_{ow} is the octanol-water partition coefficient, t is the retention time for each compound. The predicted model between t and Log K_{ow} is shown in Figure 5.7 with the experimental data from standards of BT, MPO, MP, HQ and 4NP. The retention time for compounds listed in Table 5.4 were calculated using this model, and the calculated Log K_{ow}, were listed under Predicted t (min). Data in this table were arranged in ascending order by the value of predicted retention time t. According to this table: (1) compound 13 (6.32 min), 14 (8.15 min), 16 (9.17 min), 17 (9.44 min), 18 (17.01 min), 19 (17.87 min) 21 (20.90 min) and 22 (20.90 min) are candidates for peak b, peak c, peak d, peak e and peak g in Figure 5.5, because they all have predicted retention times in the same region of the unknown peaks.

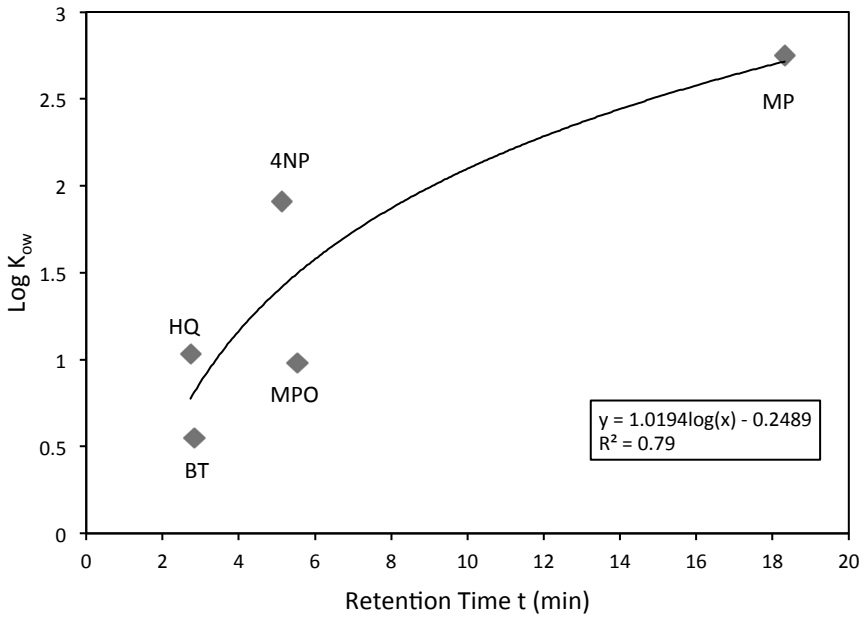

Figure 5.7 The predicted correlation between Log octanol-water coefficients Log (K_{ow}) and retention time (t) based on those of HQ, BT, MPO, 4NP and MP standards

.

Table 5.4 Predicted retention time from K_{ow} value. Log K_{ow} values and water solubility values were calculated by EPI Suite [84], and measured t values were measured by HPLC for known standards

#	Structure	Molecular weight	Log K_{ow}	Measured t (min)	Predicted t (min)	Water Solubility at 25 °C (mg/L)
1	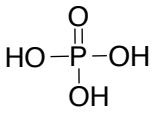	98.00	-0.77		0.60	538,600
2	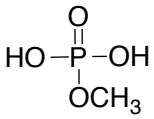	112.02	-0.71		0.64	435,900
3	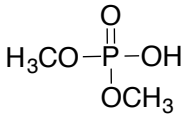	126.05	-0.66		0.67	347,200
4	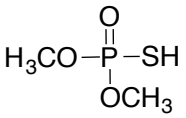	142.11	-0.51		0.77	221,800
5	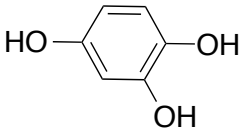	126.11	0.55	2.84	2.19	122,200
6	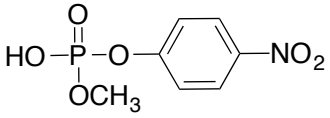	233.12	0.93		3.18	1925
7	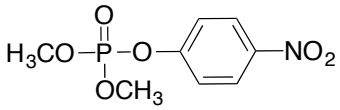	247.15	0.98	5.54	3.34	731
8	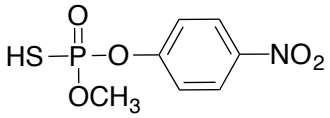	249.18	1.02		3.51	1554

Table continued on next page.

#	Structure	Molecular weight	Log K_{ow}	Measured t (min)	Predicted t (min)	Water Solubility at 25 °C (mg/L)
9	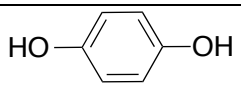	110.11	1.03	2.73	3.47	129,500
10	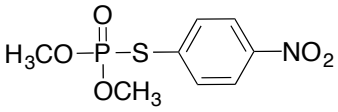	263.21	1.08		3.68	980.1
11	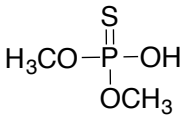	142.11	1.11		3.79	9,295
12	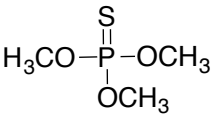	156.14	1.16		3.98	7230
13	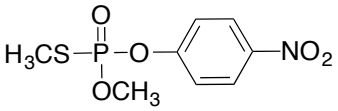	263.21	1.63		6.32	331.9
14	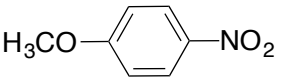	153.14	1.89		8.15	522.9
15	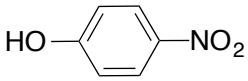	139.11	1.91	5.13	8.31	7507
16	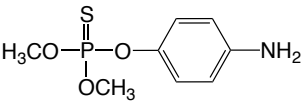	233.22	2.01		9.17	557.1
17	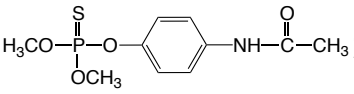	275.26	2.04		9.44	310.2
18	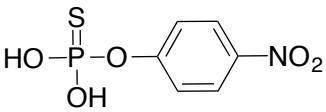	235.15	2.64		17.01	65.14
19	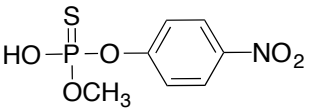	249.18	2.69		17.87	48.87

Table continued on next page.

#	Structure	Molecular weight	Log K_{ow}	Measured t (min)	Predicted t (min)	Water Solubility at 25 °C (mg/L)
20	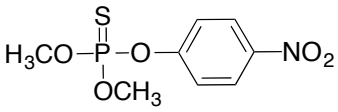	263.21	2.75	18.32	18.95	29.36
21	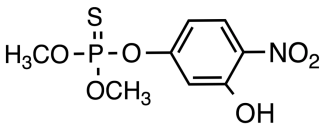	279.21	2.85		20.90	60.7
22	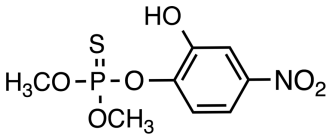	279.21	2.85		20.90	228.4

To further identify peak b, peak c, peak d, peak e, and peak g, LC-MS data were analyzed. Characteristic ions for each unidentified peak are listed in the Table 5.5. Some unknown peaks have ions with the same value and similar spectrum, especially for peak c, d and e. This makes it difficult to accurately analyze the mass spectrum for each peak and identify the compound. However, characteristic ions can still be used to further analyze the possible candidates for degradation intermediates. Compound 16, a hydrolysis intermediate with a molar mass of 233.22, is possibly corresponds to the ion $[M+H]^+$ at *m/z* 234. The molar ion at 260 is possibly corresponding to the characteristic fragment of $[(OCH_3)_2P(=S)OC_6H_4NHC(=O)]^+$. The ion $[M+H]^+$ at *m/z* 152 possibly corresponds to $HOC_6H_4NHC(=O)CH_3$. For the ion at *m/z* 248 in peak g, it might be due to the loss of OCH_3 in compound 21 or compound 22. Additionally, they are the only two compounds that exhibit higher calculated retention time (20.90 min) than MP (18.95 min) in Table 5.4. However, it is still not possible to eliminate other candidates for the degradation intermediates.

Table 5.5 LC-MS retention times (t_R), characteristic ions, and abundance of unknown peaks in the chromatogram (Figure 5.5).

Peak	t_R (min)	m/z	Abundance (%)
b	6.24	276	100
		248	20
c	7.00	260	100
		276	70
		248	50
		234	30
d	8.03	276	100
		248	70
		260	30
		234	25
		239	10
		152	8
e	8.89	260	100
		248	80
		276	60
		234	40
		239	10
g	20.07	248	100

Hydrolysis is hypothesized as the mechanism that dominates the photocatalytic degradation of methyl parathion (Scheme 5.2 – 5.4). To verify if the photocatalytic decontamination of methyl parathion in water/ethanol solvent system was predominately hydrolysis rather than oxidation and isomerization, ^{31}P NMR data was analyzed using the method developed by Seger and Maciel [70]. Based on their research, if there are isomerization intermediates (compound 10 and compound 13) produced, peaks at 22 to 27 ppm and 27 to 28 should be present; if there is oxidation, the intermediate MPO would appear as a peak at -4.8. However, only a peak around 66.3 ppm (Figure 5.8) was observed, and it is due to methyl parathion and its hydrolysis degradation intermediates which have the same phosphorus structure environment of $S=P(OR_1)(OR_2)(OR_3)$. Thus, it is concluded that hydrolysis was the major mechanism for phtocatalytic degradation of methyl parathion under the experiential condition. Based on the previous analysis of peaks for intermediates, an overall decontamination pathway was proposed for photocatalytic decontamination of methyl parathion in water/ethanol (Scheme 5.7).

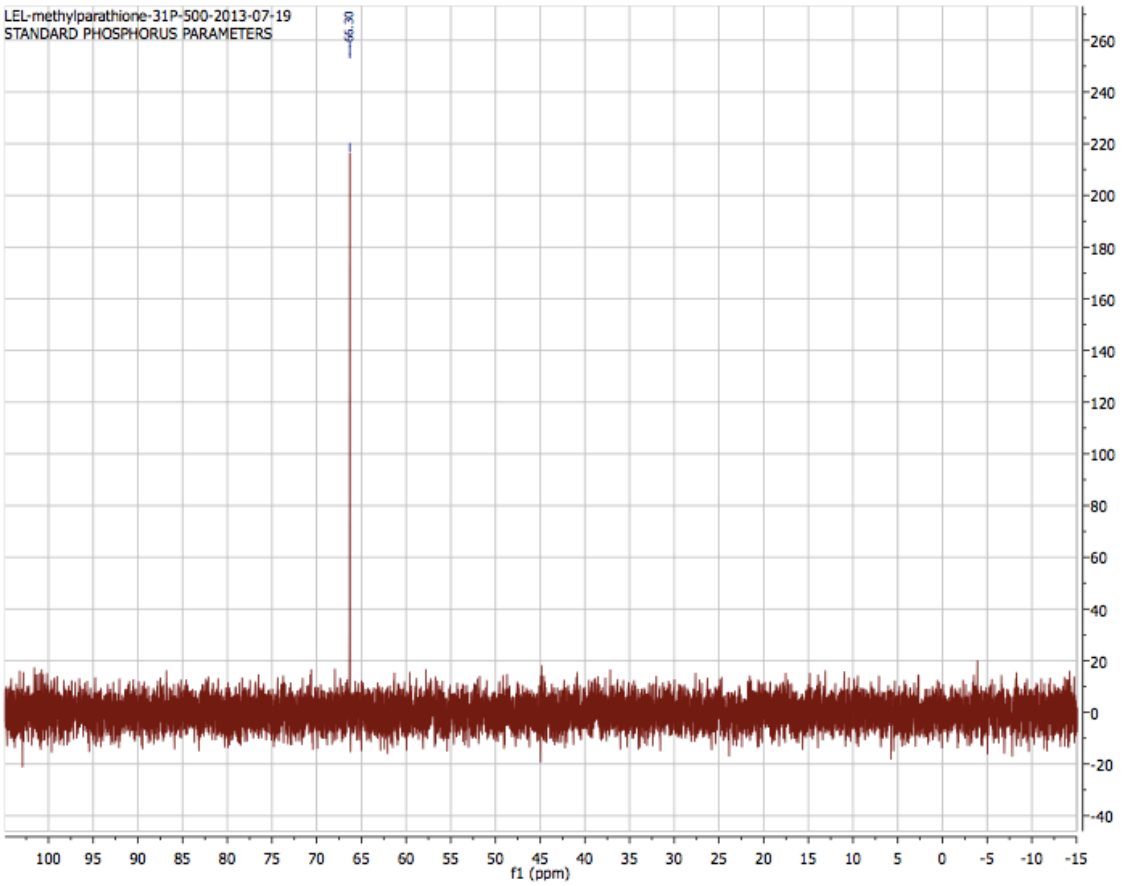

Figure 5.8 ^{31}P NMR figure for the MP solution after 1.5-hour reaction

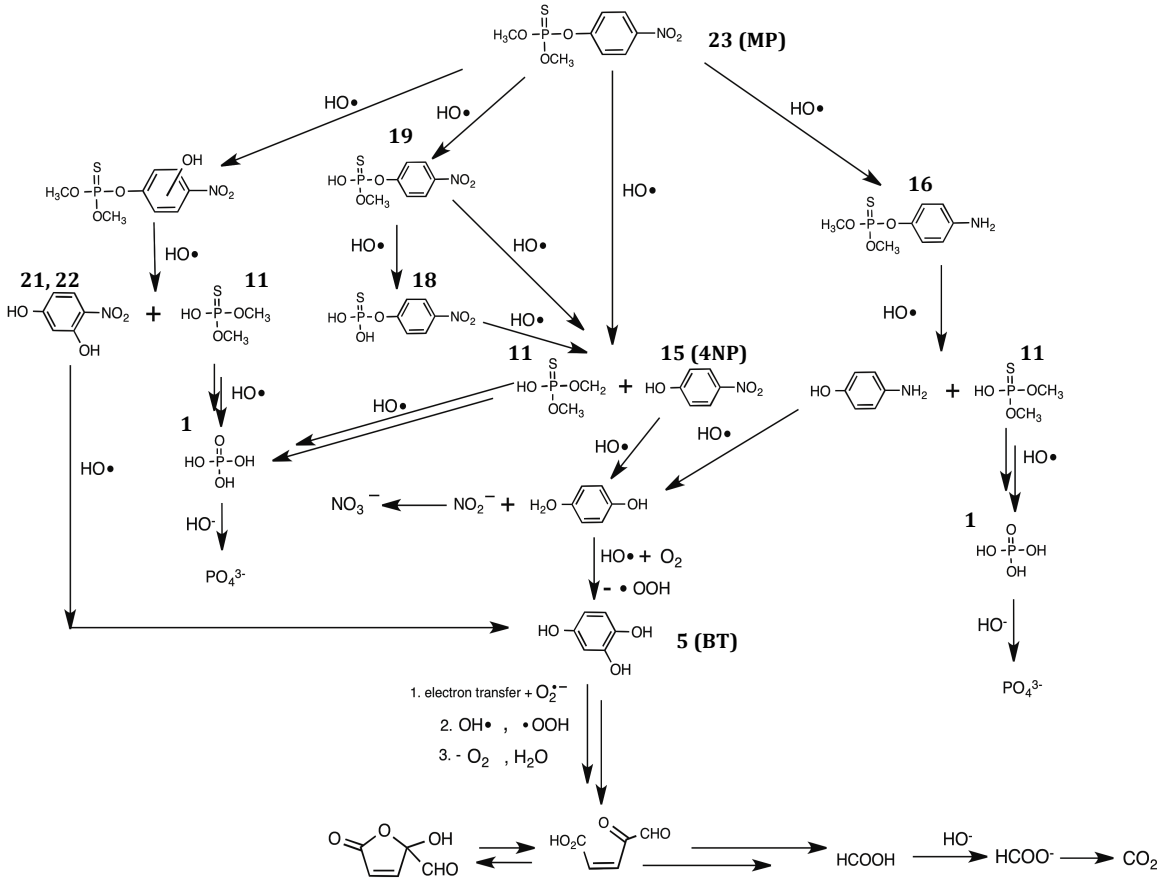

Scheme 5.7 Proposed overall decontamination pathway for photocatalytic decontamination of methyl parathion by ZnO in water/ethanol solvent system. The compounds numbers correspond to those in Table 5.4.

5.4 ZnO Nanoparticles Reuse

Data of MP amount after 2-hour reaction in UV chamber after first, second, third, and fourth use cycles are shown in Table 5.6. One-way ANOVA on these data, followed by post hoc mean comparison with Tukey correction (α= 0.05, Q= 3.29) was calculated using JMP. By comparing the amount of MP in solution after the first cycle with the MP amount after the second cycle (p-value = 0.82), the amount of MP after the first cycle with the MP amount after the third cycle (p-value = 0.75), the MP amount after the second cycle with the MP amount after the third cycle, (p-value = 0.23), it was shown that the MP amount after the first, the second, and the third cycle are not significantly different. For the fourth cycle, the amount of MP is significantly different from the MP amount after first cycle (p-value < 0.0001), second cycle (p-value < 0.0001), and third cycle (p-value < 0.0001). MP amount remaining in solution after all four cycles are significantly different from the initial amount (p-value < 0.0001). As shown in Table 5.6, it was found that the photocatalytic activity of ZnO nanoparticles was recovered for three cycles. In the fourth cycle, ZnO nanoparticles reduced the amount of MP, but the amount of MP remaining in the solution after the fourth cycle (0.20 mg) was significantly higher than the amount after the first (0.052 mg), second (0.039 mg) and the third (0.067 mg) cycles. There are two possible reasons that the degradation activity of ZnO nanoparticles for the fourth cycle was not as high as those for the first three cycles: (1) there are some hydrocarbon groups bonded on the surface of ZnO, which reduced the active surface of ZnO; (2) during

the operation process of this experiment, part of the small particles were lost, thus reduced the reaction activity. To avoid the loss of nanoparticles, immobilization of ZnO particles was achieved electrospinning fibers.

Table 5.6 MP amount in solution after photocatalytic degradation MP amount in solution after photocatalytic degradation with ZnO nanoparticles for 1, 2, 3, and 4 times for 2 hours

		Cycle number			
	Initial	1	2	3	4
MP amount (mg)	1.25	0.052 (0.0083)	0.039 (0.016)	0.067 (0.029)	0.20 (0.039)

Reported values are average amount (mg) with their standard deviations in parentheses.

5.5 Decontamination Activity And The Continued Decontamination Activity of ZnO Nanofibers on Methyl Parathion

To immobilize the nano-sized particles, ZnO was combined with PAN and electrospun into nanofibers as shown in the Figure 5.9. The mean diameter for the nanofibers was 300 nm determined by analyzing the SEM image in ImageJ software. The reactivity of methyl parathion decontamination and continued reusability experiments were conducted. Figure 5.10 shows the results after different reaction times of ZnO/PAN nanofibers on the removal of methyl parathion with UV exposure. Based on the kinetics model of catalyzed reactions [83], a model of MP amount and the reaction time (Eq. 21) was created with R^2=0.99:

$$m_{MP} = 1.275 \times e^{-9.125\times10^{-3}t} \tag{21}$$

where m_{MP} is the amount of MP remaining in sample after reaction time t. One-way ANOVA on these data showed that time had a significant effect on the amount of methyl parathion in solution after reaction in the UV chamber (F ratio = 109.11, probability > F < 0.0001). It was observed that the amount of MP remaining in the solution decreased with the increasing reaction time with ZnO/PAN nanofibers. For the reaction time of 145 hours, the MP amount variation (standard deviation = 0.19 mg) was relatively large compared with the variation for other time. This is because that the amount of MP in one of the five samples for 145 hours was unusually large (0.54 mg), while in other four samples, the MP amounts were all under 0.30 mg.

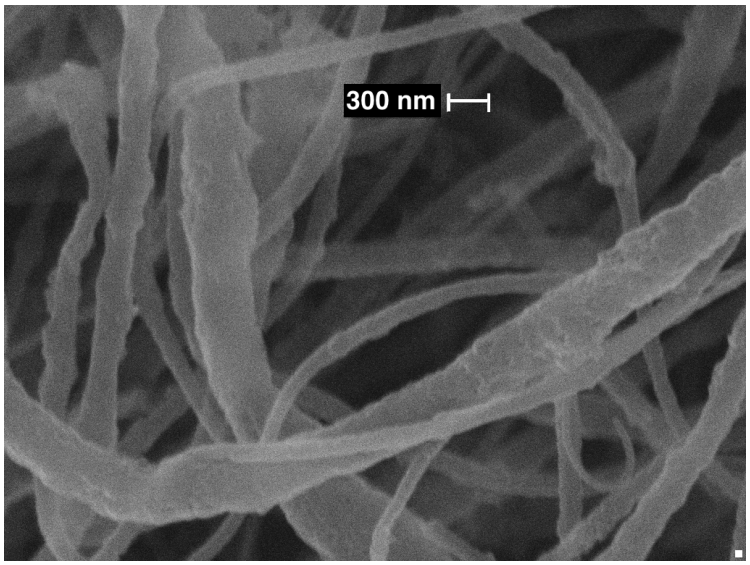

Figure 5.9 SEM image of electrospun ZnO/PAN fibers

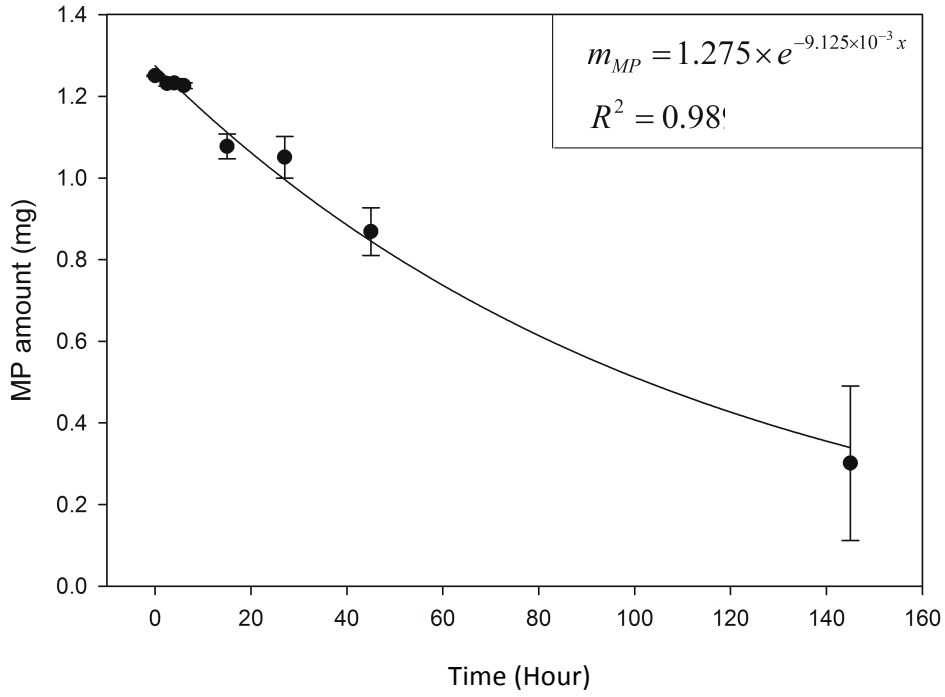

Figure 5.10 Methyl parathion amount in solution after degradation with ZnO/PAN nanofibers based on reaction time

For the reuse experiment, the same ZnO/PAN nanofibers were used as the photocatalyst and reacted with MP in solution for five reaction cycles using a washing process between reaction cycles. MP was not detected in any sample of any cycle of decontamination by ZnO/PAN nanofibers, which means that all the MP was photocatalytic decontaminated by of ZnO/PAN nanofibers after 5 days. In HPLC chromograms for the solution after every reaction cycles, only later degradation products were detected. There was no loss of activity of ZnO/PAN nanofibers after five cycles of reaction, which indicates that the immobilization of ZnO nanoparticles prevented loss of photocatalytic activity.

6. Conclusions

The photocatalytic reactivity and continued activity of methyl parathion decontamination were studied using ZnO as the catalyst. Zinc oxide proved to be very effective and efficient for MP degradation with UV. To further understand the photocatalytic mechanism in the solvent of water and ethanol, intermediates that appeared in MP degradation pathway were identified by analyzing and comparing HPLC retention time, mass spectra, UV-vis spectra, and octanol-water coefficients of possible candidates to observed intermediates. Those intermediates were all identified as hydrolysis products, thus MP photocatalytic degradation in water/ethanol was predominately hydrolysis. The reuse study on ZnO nanoparticles shows that ZnO can be reused with a slightly loss of its photocatalytic reactivity. ZnO nanoparticles were successfully immobilized in PAN by electrospinning with an average diameter of 300 nm. The study of the MP degradation by ZnO/PAN nanofibers indicates that the fibers are able to degrade MP in five days, and the degradation activity was maintained for at least five cycles.

REFERENCES

1. Szinicz, L. (2005). History of chemical and biological warfare agents. *Toxicology*, 214(3), 167-181.
2. Langston, R. D. (1992). U.S. Patent No. 5,112,666. Washington, DC: U.S. Patent and Trademark Office.
3. Katz M.G. (1989). A new approach to heat stress relief in chemical protective clothing in the proceedings of the third international symposium on protection against chemical warfare agents Stockholm. Swedish Defense Research Establishment, UMEA, Sweden 11-16, 25-31.
4. Yang, Y. C., Baker, J. A., and Ward, J. R. (1992). Decontamination of chemical warfare agents. *Chemical Reviews*, 92(8), 1729-1743.
5. Trapp, R., and Trapp, R. (1985). The detoxification and natural degradation of chemical warfare agents. Taylor & Francis.
6. Herrmann, H. W., Selwyn, G. S., Henins, I., Park, J., Jeffery, M., and Williams, J. M. (2002). Chemical warfare agent decontamination studies in the plasma decon chamber. *Plasma Science, IEEE Transactions*, 30(4), 1460-1470.
7. Bhatkhande, D. S., Pangarkar, V. G., and Beenackers, A. A. (2002). Photocatalytic degradation for environmental applications–a review. *Journal of Chemical Technology and Biotechnology*, 77(1), 102-116.
8. Rammohan, G., and N Nadagouda, M. (2013). Green Photocatalysis for Degradation of Organic Contaminants: A Review. *Current Organic Chemistry*,

17(20), 2338-2348.

9. Fujishima, A., and Honda, K. (1972). Photolysis-decomposition of water at the surface of an irradiated semiconductor. *Nature*, 238(5385), 37-38.
10. Zhang, L., Jiang, Y., Ding, Y., Povey, M., and York, D. (2007). Investigation into the antibacterial behaviour of suspensions of ZnO nanoparticles (ZnO nanofluids). *Journal of Nanoparticle Research*, 9(3), 479-489.
11. Farouk, A., Moussa, S., Ulbricht, M., Schollmeyer, E. and Textor, T. (2013). ZnO-modified hybrid polymers as an antibacterial finish for textiles. *Textile Research Journal*, 0040517513485623.
12. Chambers, J. E. and Chambers, H. W. (1991). Biotransformation of organophosphorus insecticides in mammals. *Pesticide Transformation Products Fate and Significance in the Environment*, 32-42.
13. Agency for Toxic Substances and Disease Registry (ATSDR) (2001). Toxicological Profile for Methyl Parathion. Atlanta, GA: U.S. Department of Health and Human Services, Public Health Service.
14. World Health Organization (2001) *WHO Recommended Classification of Pesticides by Hazard and Guidelines to Classification 2000–2001*. (WHO/PCS/01.4), WHO, Geneva.
15. Dastjerdi, R. and Montazer, M. (2010). A review on the application of inorganic nano-structured materials in the modification of textiles: focus on anti-microbial properties. *Colloids and Surfaces B: Biointerfaces*, *79*(1), 5-18.
16. Liu, Y., He, L., Mustapha, A., Li, H., Hu, Z. Q., and Lin, M. (2009). Antibacterial

activities of zinc oxide nanoparticles against Escherichia coli O157: H7.*Journal of applied microbiology*, *107*(4), 1193-1201.

17. Yamamoto, O. (2001). Influence of particle size on the antibacterial activity of zinc oxide. *International Journal of Inorganic Materials*, *3*(7), 643-646.
18. Yamamoto, O., Komatsu, M., Sawai, J., and Nakagawa, Z. E. (2004). Effect of lattice constant of zinc oxide on antibacterial characteristics. *Journal of Materials Science: materials in medicine*, *15*(8), 847-851.
19. Xie, Y., He, Y., Irwin, P. L., Jin, T., and Shi, X. (2011). Antibacterial activity and mechanism of action of zinc oxide nanoparticles against Campylobacter jejuni. *Applied and Environmental Microbiology*, *77*(7), 2325-2331.
20. Morton, W. J. (1902). *U.S. Patent No. 705,691*. Washington, DC: U.S. Patent and Trademark Office.
21. Cayrol, C., Sarraute, J., Tarroux, R., Redoules, D., Charveron, M., and Gall, Y. (1999). A mineral sunscreen affords genomic protection against ultraviolet (UV) B and UVA radiation: in vitro and in situ assays. *British Journal of Dermatology*, *141*, 250-258.
22. Mitchnick, M. A., Fairhurst, D., and Pinnell, S. R. (1999). Microfine zinc oxide (Z-cote) as a photostable UVA/UVB sunblock agent. *Journal of the American Academy of Dermatology*, *40*(1), 85-90.
23. Pinnell, S. R., Fairhurst, D., Gillies, R., Mitchnick, M. A., and Kollias, N. (2000). Microfine zinc oxide is a superior sunscreen ingredient to microfine titanium dioxide. *Dermatologic surgery*, *26*(4), 309-314.

24. Lee, S. (2009). Multifunctionality of layered fabric systems based on electrospun polyurethane/zinc oxide nanocomposite fibers. *Journal of Applied Polymer Science*, *114*(6), 3652-3658.
25. Kabra, K., Chaudhary, R., and Sawhney, R. L. (2004). Treatment of hazardous organic and inorganic compounds through aqueous-phase photocatalysis: A review. *Industrial & Engineering Chemistry Research*, 43(24), 7683-7696.
26. Jaeger, C. D. and Bard, A. J. (1979). Spin trapping and electron spin resonance detection of radical intermediates in the photodecomposition of water at titanium dioxide particulate systems. *Journal of Physical Chemistry*, 83(24), 3146-3152.
27. Carp, O., Huisman, C. L., and Reller, A. (2004). Photoinduced reactivity of titanium dioxide. *Progress in solid state chemistry*, 32(1), 33-177.
28. Moctezuma, E., Leyva, E., Palestino, G., and de Lasa, H. (2007). Photocatalytic degradation of methyl parathion: Reaction pathways and intermediate reaction products. *Journal of Photochemistry and Photobiology A: Chemistry*, 186(1), 71-84.
29. Fernandez-Ibanez, P., Blanco, J., Malato, S., and De Las Nieves, F. J. (2003). Application of the colloidal stability of TiO_2 particles for recovery and reuse in solar photocatalysis. *Water Research*, *37*(13), 3180-3188.
30. Doll, T. E., and Frimmel, F. H. (2005). Cross-flow microfiltration with periodical back-washing for photocatalytic degradation of pharmaceutical and diagnostic residues–evaluation of the long-term stability of the photocatalytic activity of TiO_2. *Water research*, *39*(5), 847-854.
31. Zhang, X., Du, A. J., Lee, P., Sun, D. D., and Leckie, J. O. (2008). Grafted

multifunctional titanium dioxide nanotube membrane: separation and photodegradation of aquatic pollutant. *Applied Catalysis B: Environmental*, *84*(1), 262-267.

32. Zhao, Y., Zhong, J., Li, H., Xu, N., and Shi, J. (2002). Fouling and regeneration of ceramic microfiltration membranes in processing acid wastewater containing fine TiO_2 particles. *Journal of Membrane Science*, *208*(1), 331-341.
33. Woo, D. J., Hansen, N. S., Joo, Y. L., and Obendorf, S. K. (2012). Photocatalytic self-detoxification by coaxially electrospun fiber containing titanium dioxide nanoparticles. *Textile Research Journal*, *82*(18), 1920-1927.
34. Ehrich, M. (1998). Organophosphates. *Encyclopedia of Toxicology*, *2*, 308-11.
35. Benson, P. H., Brining, D. L., and Perrin, D. W. (1973). Marine fouling and its prevention. *Marine Technology Society Journal*, *10*(1).
36. Xi, W., and Geissen, S. U. (2001). Separation of titanium dioxide from photocatalytically treated water by cross-flow microfiltration. *Water Research*,*35*(5), 1256-1262.
37. Mozia, S., Morawski, A. W., Toyoda, M., and Tsumura, T. (2009). Effect of process parameters on photodegradation of Acid Yellow 36 in a hybrid photocatalysis–membrane distillation system. *Chemical Engineering Journal*, *150*(1), 152-159.
38. Riga, A., Soutsas, K., Ntampegliotis, K., Karayannis, V., and Papapolymerou, G. (2007). Effect of system parameters and of inorganic salts on the decolorization and degradation of Procion H-exl dyes. Comparison of H_2O_2/UV, Fenton, UV/Fenton, TiO_2/UV and TiO_2/UV/H_2O_2 processes. *Desalination*, *211*(1), 72-86.

39. Lee, D. K., Kim, S. C., Cho, I. C., Kim, S. J., and Kim, S. W. (2004). Photocatalytic oxidation of microcystin-LR in a fluidized bed reactor having TiO_2-coated activated carbon. *Separation and Purification Technology*, 34(1), 59-66.
40. Chong, M. N., Vimonses, V., Lei, S., Jin, B., Chow, C., and Saint, C. (2009). Synthesis and characterisation of novel titania impregnated kaolinite nano-photocatalyst. *Microporous and mesoporous materials*, *117*(1), 233-242.
41. Zhu, H., Gao, X., Lan, Y., Song, D., Xi, Y., and Zhao, J. (2004). Hydrogen titanate nanofibers covered with anatase nanocrystals: a delicate structure achieved by the wet chemistry reaction of the titanate nanofibers. *Journal of the American Chemical Society*, *126*(27), 8380-8381.
42. Fiermans, L., Arijs, E., Vennik, J., and Maenhout-Van der Vorst, W. (1973). A combined LEED, AES and XPS study of the ZnO {0001} polar surfaces: I. LEED, AES and XPS of contaminated surfaces. *Surface Science*, *39*(2), 357-367.
43. Coppa, B. J., Fulton, C. C., Hartlieb, P. J., Davis, R. F., Rodriguez, B. J., Shields, B. J., and Nemanich, R. J. (2004). In situ cleaning and characterization of oxygen-and zinc-terminated, n-type, ZnO {0001} surfaces. *Journal of Applied Physics*, *95*(10), 5856-5864.
44. Meng, L. J., Moreira de Sá, C. P., and Dos Santos, M. P. (1994). Study of the structural properties of ZnO thin films by X-ray photoelectron spectroscopy. *Applied Surface Science*, *78*(1), 57-61.
45. Leschkies, K. S., Divakar, R., Basu, J., Enache-Pommer, E., Boercker, J. E., Carter, C. B., Kortshagen, U.R., Norris, D.J., Aydil, E. S. (2007). Photosensitization of ZnO

nanowires with CdSe quantum dots for photovoltaic devices. *Nano Letters*, *7*(6), 1793-1798.

46. Morris, R. S., and Walsh IV, M. A. (1999). *U.S. Patent No. 5,916,947*. Washington, DC: U.S. Patent and Trademark Office.
47. Harris, R., and Paxman, J. (1982). A Higher Form of Killing: The Secret Story of Gas and Germ Warfare. *London, England: Chatto & Windus Ltd*.
48. Homeland Security (2007). Guide for the Selection of Chemical, Biological, Radiological, and Nuclear Decontamination Equipment for Emergency First Responders. Preparedness Directorate Office of Grants and Training, ed2, Guide 103–06
49. Chauhan, S., Chauhan, S., D'cruz, R., Faruqi, S., Singh, K. K., Varma, S., and Karthik, V. (2008). Chemical warfare agents. *Environmental Toxicology and Pharmacology*, *26*(2), 113-122.
50. Office of the Chief of Naval Operations (1946). History of the Armed Guard Afloat, World War II. 1-15. Washington.
51. Committee On Veterans' Affairs (1994) U.S. Is Military Research Hazardous To Veterans' Health? Lessons Spanning Half A Century. U.S. Government Printing Office, Washington.
52. Bluff, P. (2007). 45 Percent Chemical Weapon convention Milestone. U.S. Army Chemical Materials Agency.
53. Conference of the States Parties (2001). Opening Statement by the Director-General to the Conference of the States Parties. OPCW, Sixteenth Session

54. Pursley, W. L. (1989). *U.S. Patent No. 6,529*. Washington, DC: U.S. Patent and Trademark Office.
55. Garner, J. B. (1920). *U.S. Patent No. 1,332,290*. Washington, DC: U.S. Patent and Trademark Office.
56. Davy Jones' College (Mar. 1944). Gas Mask Weighing Half As Much. *Popular Sciences*, p. 74.
57. Alexandroff, E. E. (1986). Saratoga: Carbon Pellet Technology in Chemical Warfare Protective Fabrics. National Defence Research Establishment, UMEA, Sweden. p 67-76
58. Alexandroff, E. E. (1989). PBI Saratoga New and Improved CWU/66p Chemical Protective Clothing System for Aircrew Application. National Defence Research Establishment, UMEA, Sweden. p 63-70
59. Boopathi, M., Singh, B., and Vijayaraghavan, R. (2008). A review on NBC body protective clothing. *Open Textile Journal*, *1*, 1-8.
60. E. Helper (1998). The New Personal Chemical Protective Suit of the U.S Military Services. National Defence Research Establishment, UMEA, Sweden p 200.
61. Morrison, R. W. (2002). Overview of current collective protection filtration technology. In *2002 NBC Defense Collective Protection Conference*.
62. Sundarrajan, S., Chandrasekaran, A. R., and Ramakrishna, S. (2010). An Update on Nanomaterials-Based Textiles for Protection and Decontamination. *Journal of the American Ceramic Society*, *93*(12), 3955-3975.
63. Li, Y. X. and Klabunde, K. J. (1991). Nano-scale metal oxide particles as chemical

reagents. Destructive adsorption of a chemical agent simulant, dimethyl methylphosphonate, on heat-treated magnesium oxide. *Langmuir*, *7*(7), 1388-1393.

64. Quin, L. D. and Duke, J. B. (2000). *A Guide to Organophosphorus Chemistry*. New York: Wiley. Vol. 2
65. Delfino, R. T., Ribeiro, T. S., and Figueroa-Villar, J. D. (2009). Organophosphorus compounds as chemical warfare agents: a review. *Journal of the Brazilian Chemical Society*, *20*(3), 407-428.
66. Nostrandt, A. C., Padilla, S., and Moser, V. C. (1997). The relationship of oral chlorpyrifos effects on behavior, cholinesterase inhibition, and muscarinic receptor density in rat. *Pharmacology Biochemistry and Behavior*, *58*(1), 15-23.
67. Abou-Donia, M. B. (1994). Organophosphorus pesticides. In Handbook of neurotoxicology, eds. L. W. Chang and R. S. Dyer. New York: Marcel Dekker, p 419–473.
68. Moctezuma, E., Leyva, E., Palestino, G., and de Lasa, H. (2007). Photocatalytic degradation of methyl parathion: Reaction pathways and intermediate reaction products. *Journal of Photochemistry and Photobiology A: Chemistry*, 186(1), 71-84.
69. Evgenidou, E., Konstantinou, I., Fytianos, K., Poulios, I., and Albanis, T. (2007). Photocatalytic oxidation of methyl parathion over TiO_2 and ZnO suspensions. *Catalysis Today*, *124*(3), 156-162.
70. Seger, M. R., and Maciel, G. E. (2006). NMR investigation of the behavior of an organothiophosphate pesticide, methyl parathion, sorbed on clays. *Environmental*

Science & Technology, *40*(2), 552-558.

71. Topalov, A., Molnár-Gábor, D., Abramović, B., Korom, S., and Peričin, D. (2003). Photocatalytic removal of the insecticide fenitrothion from water sensitized with TiO_2. *Journal of Photochemistry and Photobiology A: Chemistry*, *160*(3), 195-201.
72. Yang, Y. C., Szafraniec, L. L., Beaudry, W. T., Rohrbaugh, D. K., Procell, L. R., and Samuel, J. B. (1996). Autocatalytic hydrolysis of V-type nerve agents. *The Journal of Organic Chemistry*, *61*(24), 8407-8413.
73. Alvim, R. S., Vaiss, V. S., Leitao, A. A., and Borges Jr, I. (2013). Hydrolysis of a VX-like Organophosphorus Compound through Dissociative Chemisorption on the MgO (001) Surface. *The Journal of Physical Chemistry C*, *117*(40), 20791-20801.
74. Corradini, D. (Ed. 2). (2012). *Handbook of HPLC*. CRC Press. p. 1- 447
75. Niessen, W. M. (2012). *Liquid chromatography-mass spectrometry*. CRC Press. p. 53 - 141
76. Aguilar, C., Ferrer, I., Borrull, F., Marcé, R. M., and Barcelo, D. (1998). Comparison of automated on-line solid-phase extraction followed by liquid chromatography–mass spectrometry with atmospheric pressure chemical ionization and particle beam mass spectrometry for the determination of a priority group of pesticides in environmental waters. *Journal of Chromatography A*, *794*(1), 147-163.
77. Lacorte, S. and Barceló, D. (1996). Determination of ppt levels of OPP in groundwater by automated on-line SPE followed by LC-ESI-MS using positive and negative ion modes of operation. *Analytical Chemistry*. 68, 2464.
78. Lacorte, S. L., Jeanty, G., Marty, J. L., and Barceló, D. (1997). Identification of

fenthion and temephos and their transformation products in water by high-performance liquid chromatography with diode array detection and atmospheric pressure chemical ionization mass spectrometric detection. *Journal of Chromatography A*, 777(1), 99-114.

79. Silverstein, R. and Webster, F. (1981). *Spectrometric Identification of Organic Compounds*. John Wiley & Sons. Chapter 5: Ultraviolet Spectrometry
80. Schwarzenbach, R. P., Gschwend, P. M., and Imboden, D. M. (2005). *Environmental Organic Chemistry*. John Wiley & Sons. p. 213-238
81. Barton, A. F. (1991). *CRC Handbook of Solubility Parameters and Other Cohesion Parameters*. CRC press. p. 79-89
82. Stefanis, E. and Panayiotou, C. (2008). Prediction of Hansen solubility parameters with a new group-contribution method. *International Journal of Thermophysics*, *29*(2), 568-585.
83. P. W. Atkins (2006). *Physical Chemistry,* CRC press. p. 830-840
84. Estimation Program Interface (EPI) Suite, Syracuse Research Corp., Syracuse, NY
85. Liu, J., Wang, L., Zheng, L., Wang, X., and Lee, F. S. (2006). Analysis of bacteria degradation products of methyl parathion by liquid chromatography/electrospray time-of-flight mass spectrometry and gas chromatography/mass spectrometry. *Journal of chromatography A*, *1137*(2), 180-187